*Korean J. Chem. Eng.*, 36(10), 1688-1707 (2019)
DOI: 10.1007/s11814-019-0343-6

pISSN: 0256-1115
eISSN: 1975-7220

# Synthesis of low-cost $HNO_3$-functionalized acetylene black carbon supported Pt-Ru/$C_{AB}$ nano electrocatalysts for the application in direct ethanol fuel cell (DEFC)

**Abhay Kumar Choudhary and Hiralal Pramanik†**

Department of Chemical Engineering & Technology, Indian Institute of Technology (Banaras Hindu University), Varanasi, U.P., India

(*Received 15 February 2019 • accepted 15 July 2019*)

**Abstract**−Ethanol electrooxidation was thoroughly investigated on laboratory synthesized Pt-Ru nano electrocatalysts. Low cost acetylene black carbon functionalized by $HNO_3$ was used as support material for synthesized Pt-Ru/$C_{AB}$ electrocatalysts. The effect of synthesis methods on the major electrocatalytic properties of Pt-Ru/$C_{AB}$ electrocatalysts were studied thoroughly. The electrocatalysts Pt-Ru/$C_{AB}$ were manufactured by different chemical reduction methods. The electrocatalysts were designated as Pt-Ru/$C_{AB}$-PLM for polyol reduction and Pt-Ru/$C_{AB}$-FAM for formic acid reduction method, respectively. The electrocatalyst synthesis method and treatment of support material remarkably enhanced the catalytic performance of synthesized Pt-Ru/$C_{AB}$ electrocatalysts. The commercial Pt-Ru/C was selected as anode electrocatalyst for comparative study with the synthesis electrocatalyst in terms of performance in half cell study and in a single direct ethanol fuel cell as well. In the direct ethanol fuel cell, synthesized Pt-Ru/$C_{AB}$-PLM produced maximum open circuit voltage of 0.71 V and highest power density of 6.02 mW/cm$^2$ at a current density of 19.52 mA/cm$^2$ at the room temperature of 35 °C. Whereas, the maximum power density of 5.13 mW/cm$^2$ at a current density of 18.70 mA/cm$^2$ and open circuit voltage of 0.717 V were obtained for commercial Pt-Ru/C electrocatalyst at the same temperature (35 °C). The power density enhanced around 2.17 times when cell temperature was increased from 35 °C to 80 °C using anode electrocatalyst Pt-Ru/$C_{AB}$-PLM. The performance of synthesized Pt-Ru/$C_{AB}$-PLM is excellent for the ethanol electrooxidation and, thus, could replace commercial Pt-Ru/C.

Keywords: Pt-Ru/$C_{AB}$ Electrocatalysts, Acetylene Black, Ethanol Electrooxidation, Polyol, Cyclic Voltammetry

## INTRODUCTION

Proton exchange membranes (PEM) based fuel cell using hydrogen, methanol or ethanol as fuel at anode represent the most promising environmentally friendly technology to date. They have drawn much attention for producing electricity via simple electrochemical reactions of hydrogen-rich molecules/fuels at anode and oxidants oxygen/air at cathode [1-3]. However, hydrogen-based proton exchange membrane fuel cell (PEMFC) has some major issues, such as dehydration of Nafion® membrane beyond the temperature (T) >80 °C, which results in poor membrane conductivity. The diffusion of fuel gas $H_2$ across the solid electrolyte/Nafion® membrane to cathode side causes mixed potential. On the other hand, methanol fuel is neuro toxic, non-renewable and offers cross-over problems through membrane electrolyte. Although other aliphatic alcohols, ethylene glycol, and glycerol have fewer cross-over problems due to their larger molecular size, the electrooxidation kinetics is very slow as they have very complex molecular structures. Thus, among all aliphatic alcohols, ethanol is highly attractive as it is renewable and can be produced from biomass resources. It is also non-toxic, safer and has lower volatility than that of methanol [4,5]. Due to the larger molecular size, permeation of ethanol to the cathode side through the membrane is less compared to methanol. In addition, energy density of ethanol (8.0 kWh/kg) is more than the methanol (6.09 kWh/kg) [6,7]. The maximum energy from ethanol could be extracted through an electrochemical route if the electrooxidation reaction comes to an end with the formation of final product $CO_2$. An ethanol molecule will release 12 electrons when the electrooxidation is complete as per the anode reaction below (Eq. (1)):

$$C_2H_5OH+3H_2O\rightarrow 2CO_2+12H^++12\,e^- \quad (1)$$

Many researchers have thoroughly studied the detailed electrooxidation of ethanol in acidic medium and proposed the following scheme of reactions mechanism:

$$\text{Total oxidation: } CH_3CH_2OH\rightarrow[CH_3CH_2OH]_{ad} \rightarrow C1_{ad},\ C2_{ad}\rightarrow CO_2 \quad (2)$$

$$\text{Partial oxidation: } CH_3CH_2OH\rightarrow[CH_3CH_2OH]_{ad} \rightarrow CH_3CHO\rightarrow CH_3COOH \quad (3)$$

Here, $C1_{ad}$ and $C2_{ad}$ are the adsorbed intermediate species on the electrocatalyst sites with one or two carbon atoms. The proposed mechanisms of ethanol electrooxidation in acidic media suggest that the adsorption of ethanol followed by the formation of stable intermediate products such as acetaldehyde and acetic acid take place during partial electrooxidation of ethanol molecules [2,4,8-10].

A significant effort has been made to establish the electrooxidation reaction mechanism of ethanol and the suitable electrocatalyst to split the ethanol molecule successfully. However, it is difficult

†To whom correspondence should be addressed.
E-mail: hpramanik.che@itbhu.ac.in

to suggest the appropriate electrocatalyst to split the ethanol molecule due to its complex molecular structure consisting of C-C bonds. This C-C bond reduces the probability of molecules to cross energy hills and gives $CO_2$ as a final product with the release of 12 electrons per molecule of ethanol fuel. Thus, in most of the studies the single cell performance based on ethanol fuel is not optimistic [4].

Generally, the platinum-based bimetallic electrocatalysts (Pt-X) where X is Ru, Sn, Au, and Pd are widely investigated and suitable for ethanol splitting. In some studies, gold, rhodium, palladium have shown electrochemical activity towards ethanol. Although, only platinum-based bimetallic electrocatalysts exhibit significant electrooxidation currents, particularly in acid medium, the performance of the direct ethanol fuel cells (DEFCs) using these anode electrocatalysts is still inadequate for practical purposes [4,5,11,12]. Thus, further qualitative improvement of the anode electrocatalyst for DEFCs is necessary for the enhancement of cell performance followed by the commercialization of both, the electrocatalysts material and the developed process. Moreover, in a typical DEFC, the three-phase boundary between the supply of reactant, electrocatalyst particle, and the PEM ensure the smooth functioning of the electrode. The path between the gas diffusion layer (GDL) and electrocatalyst particle must be ensured to supply or remove electrons to or from the reaction sites. The electrically conducting nanostructured carbon black provides a path for electron conduction in the electrocatalysts layer with very low ohmic resistance. The nanostructured carbonaceous materials or carbon black as electrocatalyst support materials have been recommended as an effective and suitable ingredient to boost the electrocatalytic activity of electrocatalysts. The support materials also help in accommodating large amount of metal loading and dispersion on it and, thus, improving the access of active electrocatalyst sites during the fuel cell reactions.

Several other properties of carbon supported metal electrocatalysts like metal particle size, morphology and size distribution are greatly dependent on carbon support materials [13]. The basic characteristics for ideal support materials of electrocatalyst are (i) high electronic conductivity, (ii) high surface area to accommodate high metal loading, (iii) suitable porosity and mesoporous structure to provide good diffusion of reactants (fuels/oxidants) and reaction by-products, and (iv) the presence of sufficient surface oxygen groups to incorporate large loading of metallic nanoparticles that should favor diffusion of reactants to the active sites [3,14]. Moreover, carbon support should have well-developed and distributed pore structure with high pore volume, leading to a high surface area and better stability of electrocatalyst in acidic and alkaline medium.

Note that the support materials, mainly carbon blacks, are widely used as electrocatalyst support materials in low-temperature fuel cells. Till date, Vulcan XC-72(R) has been used as the most common electrocatalyst support inspite of its high price and unavailability [15,16]. Among all electrocatalysts support materials, Vulcan XC-72(R) is an optimal compromise between pore volume and surface area. However, Vulcan XC-72(R) has micropores of about 30% of total area, containing a large portion of active electrocatalyst which may not be accessible by the fuels ethanol and, thus, remain unutilized [1,3].

Uchida et al. [17] investigated the effect of carbon support for the synthesis of bimetallic anode electrocatalysts Pt-Ru for direct methanol fuel cells (DMFCs). The Pt-Ru electrocatalyst supported on acetylene black (AB) with the smallest specific surface area and pore size distribution in the range of 3 to 8 nm showed better performance among other carbon black support materials. Han et al. [18] performed a similar study on support material and observed that the high loading of Pt-Ru (80 wt%) alloy electrocatalyst supported on acetylene black exhibited promising cell performance for methanol fuel in acidic media in comparison to other carbon support materials. Zhiani et al. [19] reported that the performance Pt-Ru (20 : 10 wt%)/acetylene black for methanol oxidation in acidic media was superior to the commercial electrocatalyst Pt-Ru (20 : 10 wt%)/C. From this perspective, a commercial pristine/untreated carbon support acetylene black ($C_{PAB}$) was investigated due to its several good characteristics, such as moderate surface area, high conductivity, low cost, availability, and large pore volume.

It is also seen from the published literature, the method of electrocatalyst synthesis can greatly influence the composition, morphology and dispersion of the electrocatalysts, along with their electrocatalytic performance. However, very scant work can be found in the open literature on the performance comparison of electrocatalysts, synthesized by different methods. No such research has been reported in published literature to date, on functionalized acetylene black ($C_{AB}$) as carbon support material for the synthesis of Pt-Ru electrocatalysts which could effectively split ethanol molecule in half-cell and single-cell experiments, respectively.

In this paper, a thorough investigation is reported on the preparation and performance evaluation of Pt-Ru (26.35% : 13.65% by wt)/$C_{AB}$ electrocatalysts. The influence of the synthesis method on the physicochemical and electrochemical properties of synthesized Pt-Ru/$C_{AB}$ electrocatalysts was systematically evaluated. The metal nano particles were deposited on the carbon support by the impregnation method followed by the reduction with common reducing agents ethylene glycol (polyol) and formic acid, respectively. The prepared electrocatalysts were characterized using an XRD, SEM, TEM, XPS and EDX analysis. The cyclic voltammetry (CV) and chronoamperometry (CA) analyses of ethanol electrooxidation on synthesized electrocatalyst were performed to substantiate the electrocatalyst performance. Single cell experiments were also carried out to evaluate the performance of synthesized Pt-Ru (26.35% : 13.65% by wt.)/$C_{AB}$ electrocatalysts by different chemical reduction methods for its commercial application. Note that the electrocatalyst loading was kept very low in the range of 1 mg/cm$^2$ for anode and cathode both the electrodes.

## EXPERIMENTAL

### 1. Materials

The metal precursors used to prepare anode electrocatalysts were $H_2PtCl_6 \cdot 6H_2O$ (20 wt% Pt, Alfa Aesar, USA), and $RuCl_3$ (48.2 wt% Ru, Alfa Aesar, USA). Acetylene black ($S_{BET}$=75 m$^2$/g, Alfa Aesar, USA) was used as support material for synthesizing electrocatalysts. The commercial Pt-Ru (30% : 15% by wt.)/C (Alfa Aesar, USA) electrocatalyst was procured from Alfa Aesar, USA for comparison purpose. The purification and surface oxidation of pris-

tine acetylene black ($C_{PAB}$) carbon support material was by concentrated $HNO_3$ (Fisher Scientific, India). Carbon paper (TGP-H-60, Toray, USA) was used as a substrate for the painting of electrocatalyst ink to prepare the working electrodes in half-cell analysis and single cell set-up. Nafion® (DE 520, DuPont USA) dispersion was used as ionomer to make the electrocatalyst ink. Polytetrafluoroethylene (PTFE) dispersion (60 wt%, Sigma-Aldrich, Germany) was used as a binder. Ethylene glycol (Fisher Scientific, India) and formaldehyde (Fisher Scientific, India) were used as reducing agents for the electrocatalyst synthesis. Ethanol (Merck, Germany) was used as fuel. $HClO_4$ (Fisher Scientific, India) was used as electrolyte for electrochemical in half cell analysis. Isopropanol (Fisher Scientific, India) was used as a solvent. The commercial Nafion® 117 (Alfa Aesar, USA) was used as solid electrolyte in the DEFC single cell experiment. The commercial Pt (40 wt%)/High surface area carbon black ($C_{HiSPEC}$) (Alfa Aesar, USA) was used as cathode electrocatalyst.

**2. Electrocatalyst Preparation**

2-1. Fictionalization of Electrocatalyst Support/Acetylene Black

First, pristine acetylene black ($C_{PAB}$) was subjected to acid treatment with 60 wt% $HNO_3$. The treated carbon sample was then refluxed at 140 °C for 6 h under vigorous stirring. After cooling, the functionalized acetylene black ($C_{AB}$) was diluted with distilled water and filtered. The filtered $C_{AB}$ was washed thoroughly with distilled water to remove any traces of acid that were present in functionalized acetylene black. The wet acetylene black was then dried in an air oven at 80 °C for 8 h to remove free moisture [20]. The dry mass of functionalized/treated acetylene black was designated as "$C_{AB}$". The bimetallic Pt-Ru electrocatalysts, supported on pristine $C_{PAB}$ and functionalized $C_{AB}$, were prepared by ethylene glycol (polyol) and formic acid chemical reduction methods, respectively. The appropriate concentrations of the metal precursors were used to obtain a theoretical amount of Pt-Ru (26.35% : 13.65% by wt.)/$C_{PAB}$ and Pt-Ru (26.35% : 13.65% by wt.)/$C_{AB}$ electrocatalysts with Pt to Ru molar ratio of 1 : 1 metal loading on the pristine acetylene black ($C_{PAB}$) and functionalized carbon support material $C_{AB}$.

2-2. Polyol Reduction Method (PLM)

The polyol reduction method (PLM) was adopted for the electrocatalyst synthesis as proposed by Lee et al.; the detailed PLM is discussed elsewhere [21,22]. In this method, ethylene glycol is used as both a solvent and reductant of metal precursors. The required amounts of metal precursors $H_2PtCl_6{\cdot}6H_2O$ and $RuCl_3$ were taken to obtain final composition of the synthesized electrocatalysts as mentioned above. The electrocatalysts so obtained were named as Pt-Ru (26.35% : 13.65% by wt.)/$C_{PAB}$-PLM or Pt-Ru/$C_{PAB}$-PLM and Pt-Ru (26.35% : 13.65% by wt.)/$C_{AB}$-PLM or Pt-Ru/$C_{AB}$-PLM.

In another preparation, the required quantity of platinum (Pt) based metal precursor $H_2PtCl_6{\cdot}6H_2O$ was also used to synthesize Pt supported on functionalized acetylene black $C_{AB}$ i.e., Pt (40 wt%)/$C_{AB}$-PLM to evaluate the formation of Pt-Ru alloy in the synthesized bi-metallic electrocatalysts.

2-3. Formic Acid Reduction Method (FAM)

Similar to PLM, the formic acid reduction method (FAM) was adopted for electrocatalyst synthesis as proposed by Álvarez et al.; the detailed method is described elsewhere [23]. A similar amount of metal precursors $H_2PtCl_6{\cdot}6H_2O$ and $RuCl_3$ were taken in this process to get the same composition of electrocatalysts as obtained through PLM route. The obtained electrocatalysts were named as Pt-Ru (26.35% : 13.65% by wt.)/$C_{PAB}$-FAM or Pt-Ru/$C_{PAB}$-FAM and Pt-Ru (26.35% : 13.65% by wt.)/$C_{AB}$-FAM or Pt-Ru/$C_{AB}$-FAM.

**3. Preparation of Anode, Cathode, and Membrane Electrode Assembly (MEA)**

The anode and cathode electrodes were prepared using similar techniques. The complete fabrication of gas (oxidant/liquid) diffusion electrodes (GDE) is basically a two-step process. First, commercial GDL/carbon paper was coated with a thin carbon layer followed by drying in an oven at 80 °C for 1 h. Then, the carbon-coated GDL was used as a substrate to paint electrocatalyst ink, which formed a thin layer of active electrocatalyst zone. The carbon coated GDL and electrocatalyst layer combined to make an electrode shown in Fig. 1(a).

A homogeneous suspension of electrocatalyst ink composed of isopropanol, PTFE dispersion, pristine acetylene black carbon ($C_{PAB}$) powder and synthesized electrocatalyst of suitable loading was made using ultrasonication for 30 min. The electrocatalyst ink/slurry was then sprayed onto the carbon paper GDL to form the

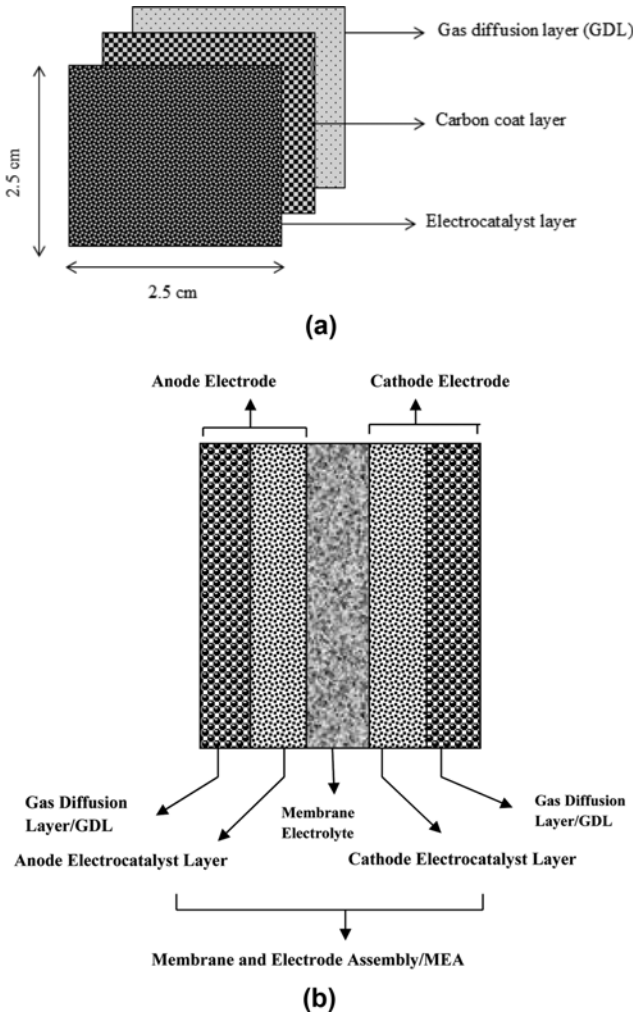


**Fig. 1. (a) Three layer composite of the fabricated electrode. (b) Schematic of the clamped MEA.**

electrocatalyst layer. The composite structure of the electrocatalyst layer and GDL was then dried in an air oven at 80 °C for 1 h. Finally, the dried electrode was sintered in a vacuum oven at 300 °C for 3 h to get the porous structure of the electrode. This improved the active surface of the electrode with a better mass transfer from bulk to active the electrocatalyst layer. The dimension of active electrodes, i.e., anode and cathode electrodes, was 2.5 cm×2.5 cm. The fabricating technique for anode and cathode is similar, except for the electrocatalyst used. The MEA was prepared by clamping technique [24]. The anodes were fabricated using synthesized Pt-Ru/$C_{PAB}$-PLM or Pt-Ru/$C_{PAB}$-FAM or Pt-Ru/$C_{AB}$-PLM or Pt-Ru/$C_{AB}$-FAM or commercial Pt-Ru/C with electrocatalyst loading of 1 mg/cm$^2$. The cathode was developed from the commercial Pt (40 wt%)/$C_{HiSPEC}$ of 1 mg/cm$^2$ loading in all MEA. The MEA was fabricated, keeping the commercial Nafion® 117 membranes/electrolyte between the sintered anode and cathode using clamping method without any hot pressing for the use in single cell DEFC (Fig. 1(b)).

**4. Physical Characterization**

The crystalline structure of electrocatalyst support material and supported electrocatalysts were investigated using the powder XRD technique. The XRD patterns were generated by an XRD diffractometer (Rigaku Ultima IV, Germany) containing nickel-filtered Cu K$\alpha$ radiation source ($\lambda$=0.154056 nm), maintaining the tube voltage at 40 kV and tube current at 15 mA. The amount of electrocatalyst sample taken was 30 mg in order to obtain a uniform distribution of the sample. The $2\theta$ angles were varied from 20° to 80° at a scan rate of 5° min$^{-1}$ with a 0.02° angular resolution.

The FTIR spectra of the carbon support material were recorded using Nicholet iS5 (Thermo Electron) spectrometer in the reflectance mode at room temperature. At first, the sample (KBr pellet) was prepared by mixing of the appropriate amount of carbon powder support with potassium bromide (KBr) powder.

The pH of pristine and functionalized acetylene black carbon support material ($C_{PAB}$ and $C_{AB}$) was measured with a pH-meter CL 54$^+$(TOSHCON) in an aqueous slurry containing 1 g of carbon black powder. The slurry was made using ultrasonic water followed by another mixing with magnetic stirrer. The pH of the suspension was measured at steady state.

TEM analyses of synthesized electrocatalysts were performed with Tecnai G2 20 Twin (FEI Company, USA) microscope to investigate the particle size distribution and mean particle size. TEM. The electrocatalyst samples were prepared by dispersing in ethanol using ultrasonic water bath. The electrocatalyst sample was applied on carbon coated Cu grid using a micro pipette. The sample grid was then dried in a vacuum oven at 60 °C for 4 h.

The surface morphology of the carbon support material and dispersed electrocatalysts was examined by SEM. The elemental composition at the surface of the electrocatalyst was investigated by EDX using Octane Plus SDD detector (EDAX Inc.) coupled with SEM instruments (Nova Nano SEM 450, FEI Company U.S.A).

The XPS analysis of the electrocatalysts was performed with a spectrometer (AMICUS) attached to Mg-K$\alpha$ (1,253.6 eV) X-ray radiation source (Shimadzu Group Company, Japan). The binding energies were calibrated with reference to the C (1s) peak value of 284.6 eV with an accuracy of ±0.2 eV. The XPS spectra of the Pt (4f) and Ru (3d) signals were analyzed by spin-orbit splitting with a Shirley background function and Gaussian-Lorentzian function using the XPS PEAK 4.1 software. The surface concentration of different oxidation states of Pt and Ru in the electrocatalyst samples was estimated from the surface area of the respective Gaussian-Lorentzian peaks.

**5. Electrochemical Measurements in Half Cell**

The electrocatalytic activity of all the anode electrocatalysts was evaluated by cyclic voltammetry (CV) and chronoamperometry (CA) techniques using a three electrode cell assembly (PGSTAT 204, Autolab Netherland) at 35 °C.

The carbon paper/GDL, coated with active electrocatalyst and long platinum wire, was chosen as working and the counter electrode, respectively. The reference electrode used was Ag/AgCl in saturated KCl. The working electrode was prepared by using electrocatalyst ink made of 2 mg of electrocatalysts in 5 µL Nafion® (5 wt%) solution and a drop of PTFE dispersion. The electrocatalyst ink was prepared in a similar manner as adopted for anode and cathode electrocatalyst ink preparation. The dispersed electrocatalyst ink was coated on the tip of a long strip of carbon paper of 0.25 cm$^2$ area in single side as shown in Fig. 2. All the electrochemical measurements were performed in an acidic solution containing 0.5 M $HClO_4$ and 1.0 M ethanol. Nitrogen gas was purged through the electrolyte solution for 30 min before each experiment to remove dissolve $O_2$ from the electrolyte solution, which could hinder the electrooxidation of ethanol fuel.

**6. DEFC Study**

The DEFC single cell tests were carried out using MEA with a geometric active electrode area of 6.25 cm$^2$ MEA clamped between two stainless steel blocks with serpentine flow channels of dimension 2 mm×2 mm (depth×width) for the reactant flow. PTFE tape was used on both sides of the MEA for insulation and leakage prevention. An aqueous solution of 1 M ethanol fuel was fed into the anode by a peristaltic pump (Electrolab, India) at a fixed flow rate of 1.2 ml/min, and humidified oxygen gas was supplied to the cathode side from cylinder at a flow rate of 60 ml/min. The steady state voltage-current (V-I) data of DEFC were collected using DC electronic load (K-PAS Instronic Engineers India pvt. ltd.). All the DEFC tests were performed at 35 °C and 1 bar (absolute) pressure for both side anode and cathode, respectively.

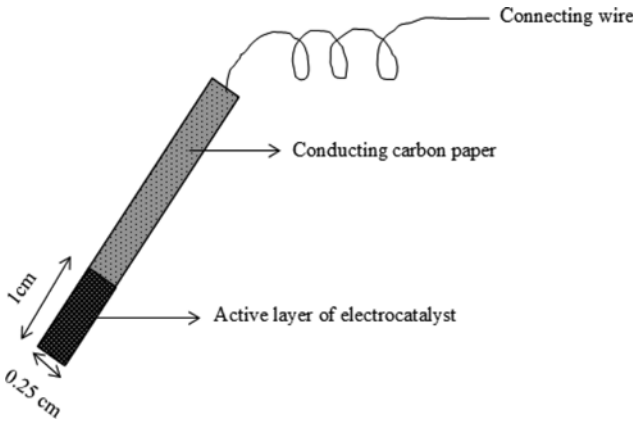


**Fig. 2. Working electrode for electrochemical characterization.**

## RESULTS AND DISCUSSION

### 1. Characterization of the Acetylene Black Carbon Support

As discussed earlier, the nature of carbon support material plays a key role in the synthesis of supported electrocatalyst for fuel cell. de la Fuente et al. reported that carbonaceous materials treatment with concentrated $HNO_3$ is an effective acid reagent for creating surface functional groups for nanoparticle anchoring sites, hydrophilicity and dissolving the remaining impurities [25]. The pH of the aqueous slurry of nitric acid functionalized carbon black ($C_{AB}$) support decreased considerably (pH=3.2) compared to that pristine acetylene black carbon ($C_{PAB}$) support (pH=8.12). The drastic decrease in pH of functionalized carbon black ($C_{AB}$) support indicates that sufficient acidic functional groups (carboxylic groups) were introduced after acidic treatment.

The XRD patterns of pristine acetylene black ($C_{PAB}$) and functionalized acetylene black carbon ($C_{AB}$) support are presented in Fig. 3(a)-(b). The XRD patterns of $C_{PAB}$ and $C_{AB}$ support show two common peaks of both the samples. It was also observed from the Fig. 3(a)-(b) that there are two peaks at the $2\theta$ value of 25.54° (002), and 42.65° (100), which indicate the characteristic diffraction pattern of the graphitic structure of the acetylene black support material (JCPDS card no. 34-1832). The first intense peak around $2\theta$ of 25.56° refers to the high degree of graphitization (002) facet of support material [26].

The XRD results of acetylene black support material as listed in Table 1 indicate that the interplanar spacing of $C_{AB}$ is 0.3513 nm due to random planes orientations compares to the graphite interplanar spacing of 0.335 nm. The existence of $sp^2$ carbon-bonded graphite crystals of carbon support $C_{PAB}$ and $C_{AB}$ confirms that acetylene black has a turbostratic structure [27]. After the acid treatment with concentrated nitric acid, the (002) peak of acetylene black carbon support became sharper and intense. The functionalized acetylene black ($C_{AB}$) shows a smaller $d_{002}$ spacing value of 0.3473 nm and larger crystallite size ($L_c$) of 3.37 nm in comparison to pristine acetylene black carbon ($C_{PAB}$).

Fig. 4(a)-(b) shows SEM images of pristine acetylene black ($C_{PAB}$) and functionalized acetylene black carbon ($C_{AB}$). In the SEM images the carbon support is of spherical morphology consisting of carbon nano spheres with size in the range of 40 to 60 nm. Pristine acetylene black carbon ($C_{PAB}$) consisted of agglomerated spherically shaped carbon nanospheres with cross linked structure and formed

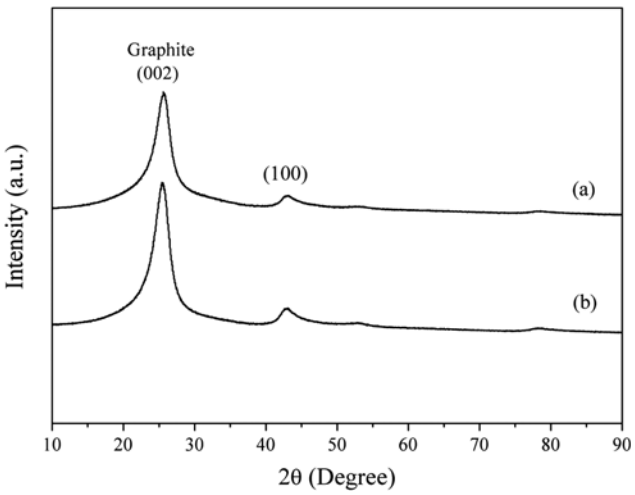


**Fig. 3. XRD pattern of (a) pristine acetylene black carbon ($C_{PAB}$) and (b) functionalized acetylene black carbon ($C_{AB}$) support.**

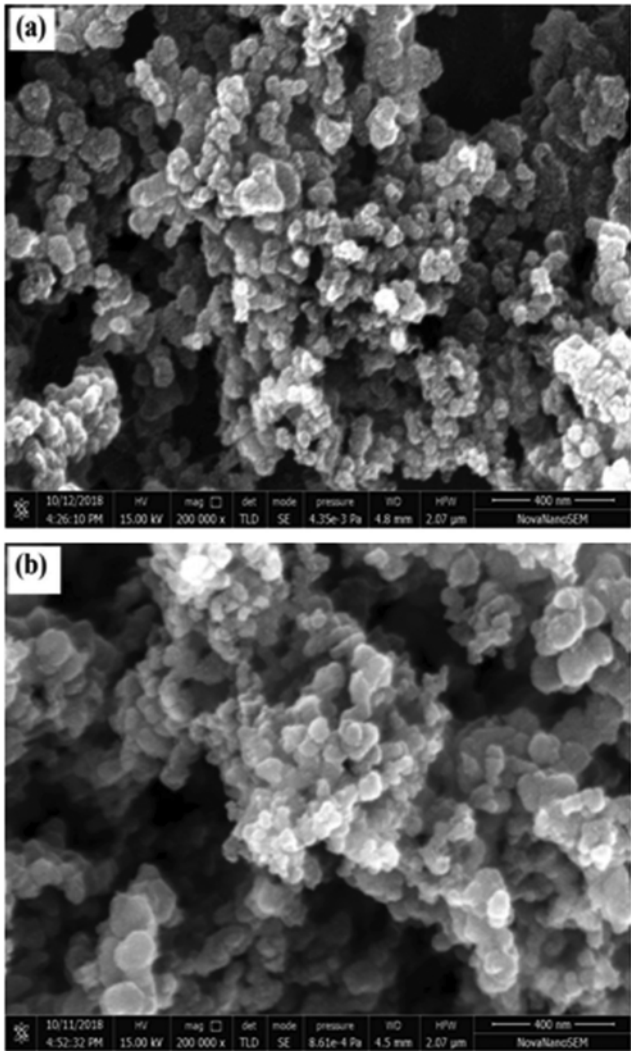


**Fig. 4. SEM images of (a) pristine acetylene black carbon ($C_{PAB}$) (b) functionalized acetylene black carbon ($C_{AB}$) support.**

**Table 1. Physical properties of acetylene black support material derived from XRD patterns**

| Carbon support | (002) Position | $d_{002}$ Spacing (nm) | FWHM peak | Crystallite size ($L_c$) |
|---|---|---|---|---|
| Pristine acetylene black carbon ($C_{PAB}$) | 25.34 | 0.3513 | 3.09 | 2.82 |
| Functionalized acetylene black carbon ($C_{AB}$) | 25.62 | 0.3473 | 2.53 | 3.37 |

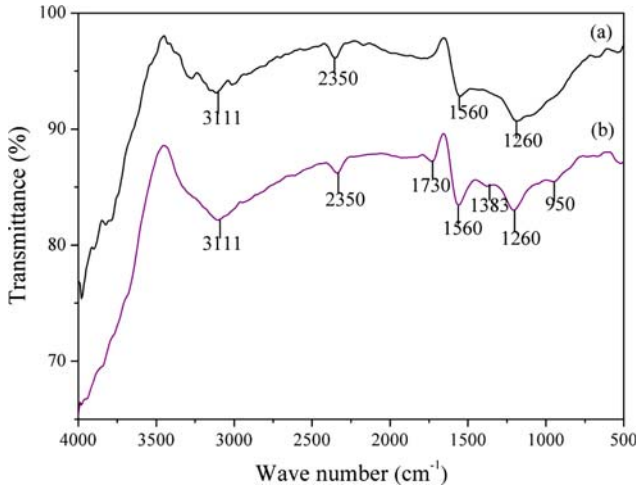


**Fig. 5. FTIR spectroscopy of (a) pristine acetylene black carbon ($C_{PAB}$) and (b) functionalized acetylene black carbon ($C_{AB}$) support.**

aggregates in the form of clusters or a steric specific chain structure. The morphological change in the functionalized acetylene black carbon ($C_{AB}$) is not significant in comparison to pristine acetylene black carbon ($C_{PAB}$), except a minute change in particle size (Fig. 4(b)). These results suggest that the treatment of carbon support with $HNO_3$ does not affect their physical morphology severely. However, it modifies their surface chemical properties such as hydrophilicity and surface functional groups, which is discussed in the following section.

The FTIR is a very useful analysis technique which detects various characteristic functional groups present in the carbon support samples, i.e., $C_{PAB}$ and $C_{AB}$, respectively. Fig. 5(a)-(b) shows the FTIR spectra of $C_{PAB}$ and $C_{AB}$ using FTIR in the wavelength range of 500-4,000 $cm^{-1}$. Both the samples of carbon support show four common peaks located at about 3,111 $cm^{-1}$, 2,350 $cm^{-1}$, 1,560 $cm^{-1}$ and 1,206 $cm^{-1}$ are attributed to the O-H, $CO_2$, C=C, and CO-H functional groups, respectively [28-30]. Additional three peaks in functionalized acetylene black carbon ($C_{AB}$) surface at 1,730 $cm^{-1}$, 1,383 $cm^{-1}$ and 950 $cm^{-1}$ are ascribed to the oscillation of carboxylic groups (C=OOH), O-H bending deformation in carboxylic acid groups and C-H out of plane deformation, respectively [27]. It is evident from Fig. 5(b) and Table 2 that sufficient acidic functional groups have been introduced after the acid treatment on the surface of acetylene black carbon support. These created oxygen-containing groups on the surface of functionalized carbon support ($C_{AB}$) resulting in hydrophilicity and anchoring sites to form complexes with different metal ions of platinum and ruthenium.

**2. Characterization of Electrocatalysts**

2-1. SEM Analysis

The surface morphology of the electrocatalysts were thoroughly examined via SEM and their images are presented in Fig. 6(a)-(e). From Fig. 6(a)-(e), the electrocatalyst particles are of nano-range with uniform size. The uniformity is more prominent in the SEM images for the synthesized electrocatalysts Pt-Ru/$C_{AB}$-PLM (Fig. 6(c)) and commercial electrocatalyst Pt-Ru/C (Fig. 6(e)). The SEM analysis also confirms that the particle sizes are in good agreement with the average crystallite size calculated from XRD analysis and average particle size from TEM analysis. The SEM images also confirm that the synthesized electrocatalysts are porous, which could facilitate mass transport from the bulk phase to the active electrocatalysts sites.

2-2. XRD Analysis

The XRD analysis provides the bulk structural information of the electrocatalyst and its support material. Fig. 7(a)-(f) presents the XRD patterns, mainly crystallographic structures of the synthesized and commercial electrocatalysts of the electrocatalysts, respectively. The first broad diffraction peaks at $2\theta$=25.5° were observed for Pt-Ru/$C_{PAB}$-PLM, Pt-Ru/$C_{PAB}$-FAM, Pt-Ru/$C_{AB}$-PLM, Pt-Ru/$C_{AB}$-FAM and Pt/$C_{AB}$-PLM electrocatalysts due to assigned (002) graphite crystalline plane of acetylene black carbon ($C_{AB}$) support material with hexagonal structure. However, the diffraction peak of carbon support material is not found in the case of commercial Pt-Ru/C electrocatalyst because the peak intensity of support material which is generally Vulcan XC-72R gives less intense due to its lower crystallinity grade, compared to the intensity of Pt-Ru metal peak [31]. The XRD patterns of all the electrocatalysts (Fig. 7(a)-(e)) display Pt-Ru alloy diffraction peaks at around 40°, 47° and 68° are attributed to Pt (1 1 1), Pt (2 0 0), and Pt (2 2 0), respectively. This indicates the typical character of the face-centered cubic (fcc) crystalline structure of platinum (Pt). The shift of the Pt peaks to the higher angles is found in the synthesized electrocatalyst due to the presence of Pt-Ru alloy. The XRD pattern of commercial Pt-Ru/C (Fig. 7(e)) electrocatalyst shows broader peaks as compared to synthesized Pt-Ru/$C_{AB}$-PLM and Pt-Ru/$C_{AB}$-FAM. Similar trend was also observed for commercial Pt-Ru/C in comparison to Pt-Ru/$C_{PAB}$-PLM and Pt-Ru/$C_{PAB}$-FAM. Broader peaks of commercial Pt-Ru/C electrocatalyst may be due to its lower

**Table 2. Comparison and shifting of bands data of pristine ($C_{PAB}$) and functionalized acetylene black carbon ($C_{AB}$) support in FTIR analysis**

| Stretching or bending functional groups | Wave number ($cm^{-1}$) | |
|---|---|---|
| | Pristine acetylene black carbon ($C_{PAB}$) | Functionalized acetylene black carbon ($C_{AB}$) |
| C-H, out of plane deformation | … | 950 |
| C-OH stretching vibrations | 1206 | 1206 |
| O-H bending deformation in carboxylic acid | … | 1383 |
| C=C stretching vibrations of $C_{AB}$ backbones | 1560 | 1560 |
| C=O stretching in carboxylic groups | … | 1730 |
| $CO_2$ signal | 2350 | 2350 |
| O-H group | 3111 | 3111 |

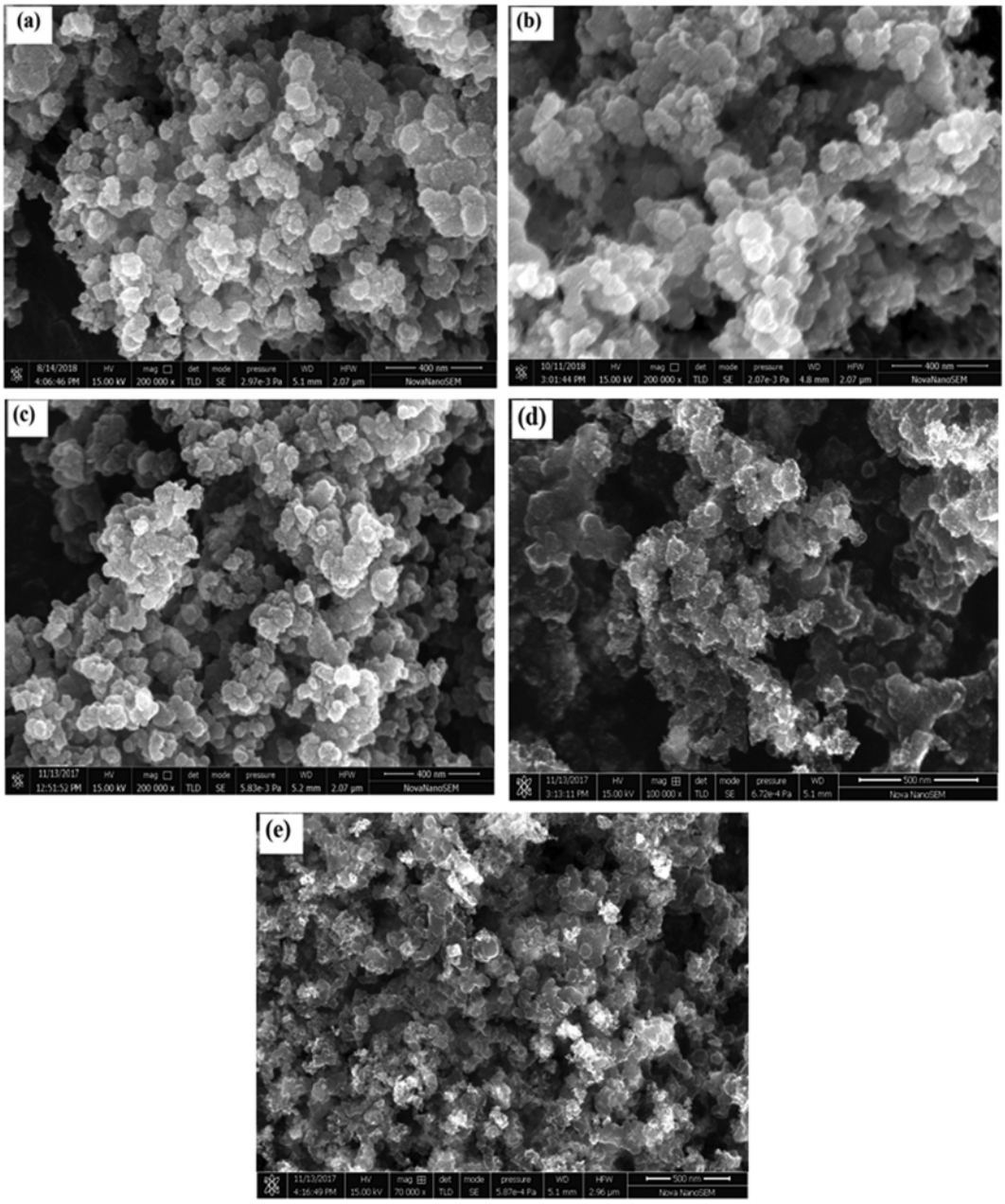


**Fig. 6. SEM images of (a) Pt-Ru/$C_{PAB}$-PLM, (b) Pt-Ru/$C_{PAB}$-FAM, (c) Pt-Ru/$C_{AB}$-PLM, (d) Pt-Ru/$C_{AB}$-FAM and (e) commercial Pt-Ru/C.**

crystallinity and smaller particles having lattice strain.

However, no diffraction peak for Ru hexagonal structure was detected in the XRD pattern of electrocatalysts, indicating its presence in the amorphous state either in the form metallic ruthenium or ruthenium oxides [32,33]. The lattice parameters (Table 3) of all the electrocatalysts are smaller than that of Pt/C (JCPDS # 040802, $a_{fcc}$=0.3915 nm) due to the formation of a Pt-Ru solid solution [34]. The ruduction in lattice parameter of Pt crystal structure reveals the incorporation of secondary smaller atomic sized Ru metal ($R_{Pt}$=1.39 Å and $R_{Ru}$=1.34 Å) into the Pt crystal to form Pt-Ru solid alloy solution. This could result in the contraction of Pt lattice parameter in Pt-Ru bimetallic supported electrocatalysts.

The average crystallite sizes ($d_c$) of Pt-Ru bimetallic supported electrocatalysts were calculated based on the broadening of the Pt (2 2 0) peak using the Debye-Scherrer equation as follows [19,35,36].

$$d_c = \frac{0.9\lambda}{\beta\cos\theta} \tag{4}$$

The metal surface area (SA) of the electrocatalyst was calculated from Eq. (5):

$$SA = \frac{60{,}000}{\rho_{Pt\text{-}Ru} d_p} \tag{5}$$

$$\rho_{Pt\text{-}Ru} = X_{Pt} \times \rho_{Pt} + X_{Ru} \times \rho_{Ru} \tag{6}$$

where $d_c$ is the average crystallite size (nm), k is a coefficient (0.9),

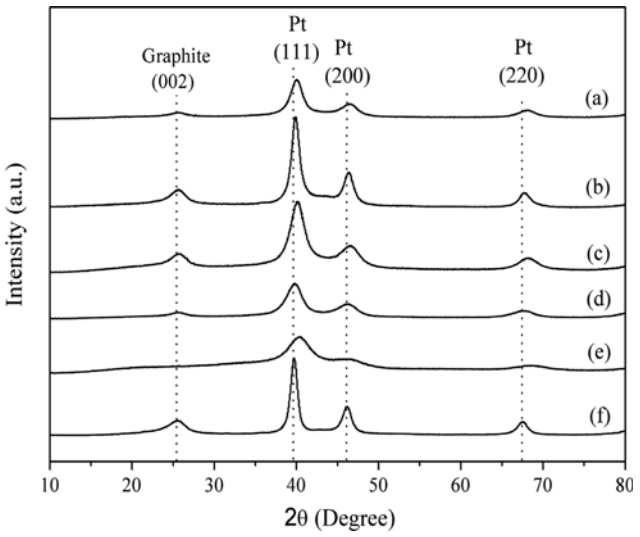


**Fig. 7. XRD patterns of (a) Pt-Ru/$C_{PAB}$-PLM, (b) Pt-Ru/$C_{PAB}$-FAM, (c) Pt-Ru/$C_{AB}$-PLM, (d) Pt-Ru/$C_{AB}$-FAM, (e) commercial Pt-Ru/C and (f) Pt/$C_{AB}$-PLM electrocatalysts.**

$\lambda$ is the wave-length of X-ray radiation (0.154056 nm), $\beta$ is the full width half-maximum (in radians) of respective diffraction peak, $\theta$ is the angle at Pt (220) position of peak, *SA* is the surface area ($m^2$/g), $d_p$ is the average particle size (nm), $\rho_{Pt\text{-}Ru}$ is the density of Pt-Ru alloy nano particles, $\rho_{Pt}$ is the density of Pt metal (21.4 g $cm^{-3}$), $\rho_{Ru}$ is the density of Ru metal (12.3 g $cm^{-3}$), and $X_{Pt}$ and $X_{Ru}$ are the wt% of Pt and Ru in the electrocatalyst, respectively.

The diffraction peaks of Pt (220) from the XRD patterns were considered to calculate the average crystallite size and lattice parameter of Pt [37,38]. The composition of the supported Pt-Ru alloy electrocatalysts were calculated by the shift of Pt-Ru diffraction peaks, i.e., the variation of the lattice parameter $a_{Pt\text{-}Ru/C}$ from the XRD patterns, which is based on Vegard's law [39]. The lattice parameter ($a_{Pt\text{-}Ru/C}$) of Pt-Ru alloy electrocatalyst was used to calculate Ru atomic fraction $x_{Ru}$ (<0.7) using the relationship of Vegard's law [40].

$$a_{Pt\text{-}Ru/C}=a_{Pt/C}-k\,x_{Ru} \tag{7}$$

where $a_{Pt/C}$ and $a_{Pt\text{-}Ru/C}$ are the lattice parameter of Pt/C and the Pt–Ru/C alloyed electrocatalyst, respectively. The value of $a_{Pt/C}$ is 0.3915 nm and the value of constant k is 0.0124 nm were taken from published literature [34,36].

The amount of alloyed ruthenium $Ru_{al}$ in the Pt-Ru/C alloy electrocatalysts was calculated using the equation below [36]:

$$Ru_{al}=\frac{x_{Ru}}{\left[(1-x_{Ru})\left(\frac{Ru}{Pt}\right)_{nom}\right]} \tag{8}$$

where, $\left(\frac{Ru}{Pt}\right)_{nom}$ represents the nominal atomic ratio of Ru to Pt and $x_{Ru}$ is the atomic content of alloyed Ru fraction in the Pt-Ru/C alloy electrocatalysts. The relative data calculated from XRD diffraction patterns by Debye-Scherrer (Eq. (4)) and Vegard's law formula (Eqs. (7) and (8)) are presented in Table 3.

It is clearly seen from Table 3 that the average crystallite size of all the synthesized bi-metallic electrocatalysts lies in the range of 3.4 nm to 5.8 nm. The average crystallite size obtained for the synthesized electrocatalysts supported on pristine acetylene black $C_{PAB}$, i.e., Pt-Ru/$C_{PAB}$-PLM and Pt-Ru/$C_{PAB}$-FAM is larger than that of the functionalized acetylene black $C_{AB}$ supported electrocatalysts Pt-Ru/$C_{AB}$-PLM and Pt-Ru/$C_{AB}$-FAM, respectively. The calculated average crystallite sizes ($d_c$) of the synthesized Pt-Ru/$C_{PAB}$-PLM and Pt-Ru/$C_{PAB}$-FAM electrocatalysts were 3.8 nm and 5.8 nm, respectively. It may be due to lack of oxygenated species on the surface of pristine acetylene black $C_{PAB}$. The alloying degree of Ru for the synthesized Pt-Ru/$C_{PAB}$-PLM and Pt-Ru/$C_{PAB}$-FAM electrocatalysts are 31.93 wt% and 26.58 wt%, which are lower than the Pt-Ru/$C_{AB}$-PLM (37 wt%) and Pt-Ru/$C_{AB}$-FAM (34 wt%), respectively. Whereas, lower average crystallite size was obtained for the synthesized electrocatalyst Pt-Ru/$C_{AB}$-FAM with the Ru alloying of about 34.04 wt%. Although, the particle size is little larger for Pt-Ru/$C_{AB}$-PLM (3.6 nm) than electrocatalyst Pt-Ru/$C_{AB}$-FAM (3.4 nm) and commercial Pt-Ru/C electrocatalyst (2.8 nm), the polyol method (Pt-Ru/$C_{AB}$-PLM) results in higher Ru alloying of 37.0 wt% with Pt noble metal. The alloying of Ru with Pt atom plays a very crucial role in electrooxidation of ethanol fuel. Thus, synthesized Pt-Ru/$C_{AB}$-PLM electrocatalyst is expected to perform excellently and produce comparable results with the commercial electrocatalyst Pt-Ru/C. Note that the single metal electrocatalyst Pt/$C_{AB}$-PLM resulted in the largest crystallite size of 6 nm. The TEM of synthesized electrocatalysts was also performed to verify the results analysis of XRD of synthesized electrocatalysts, which is discussed in the following section.

2-3. TEM Analysis

Fig. 8(a)-(e) shows the typical TEM images of electrocatalyst and their metal particle size distribution. The average particle sizes and histograms of the size distribution of metal nanoparticles were estimated by counting the diameter of 150 metal nanoparticles in

**Table 3. Data calculated from XRD patterns by Debye Scherrer formula and Vegard's law**

| Electrocatalysts | Average crystallite size ($d_c$) by XRD (nm) | Lattice parameter $a_{(Pt\text{-}Ru/C)}$ (nm) | Pt (2 2 0) position (Deg.) | Ru fraction ($x_{Ru}$) | Alloyed Ru (wt%) |
|---|---|---|---|---|---|
| Pt-Ru/$C_{PAB}$-PLM | 3.8 | 0.3885 | 68.20 | 0.242 | 31.93 |
| Pt-Ru/$C_{PAB}$-FAM | 5.8 | 0.3889 | 68.10 | 0.210 | 26.58 |
| Pt-Ru/$C_{AB}$-PLM | 3.6 | 0.3883 | 68.24 | 0.270 | 37.0 |
| Pt-Ru/$C_{AB}$-FAM | 3.4 | 0.3884 | 68.22 | 0.254 | 34.04 |
| Commercial Pt-Ru/C | 2.8 | 0.3877 | 68.35 | 0.310 | 44.73 |
| Pt/$C_{AB}$-PLM | 6.0 | 0.3915 | 67.60 | --- | --- |

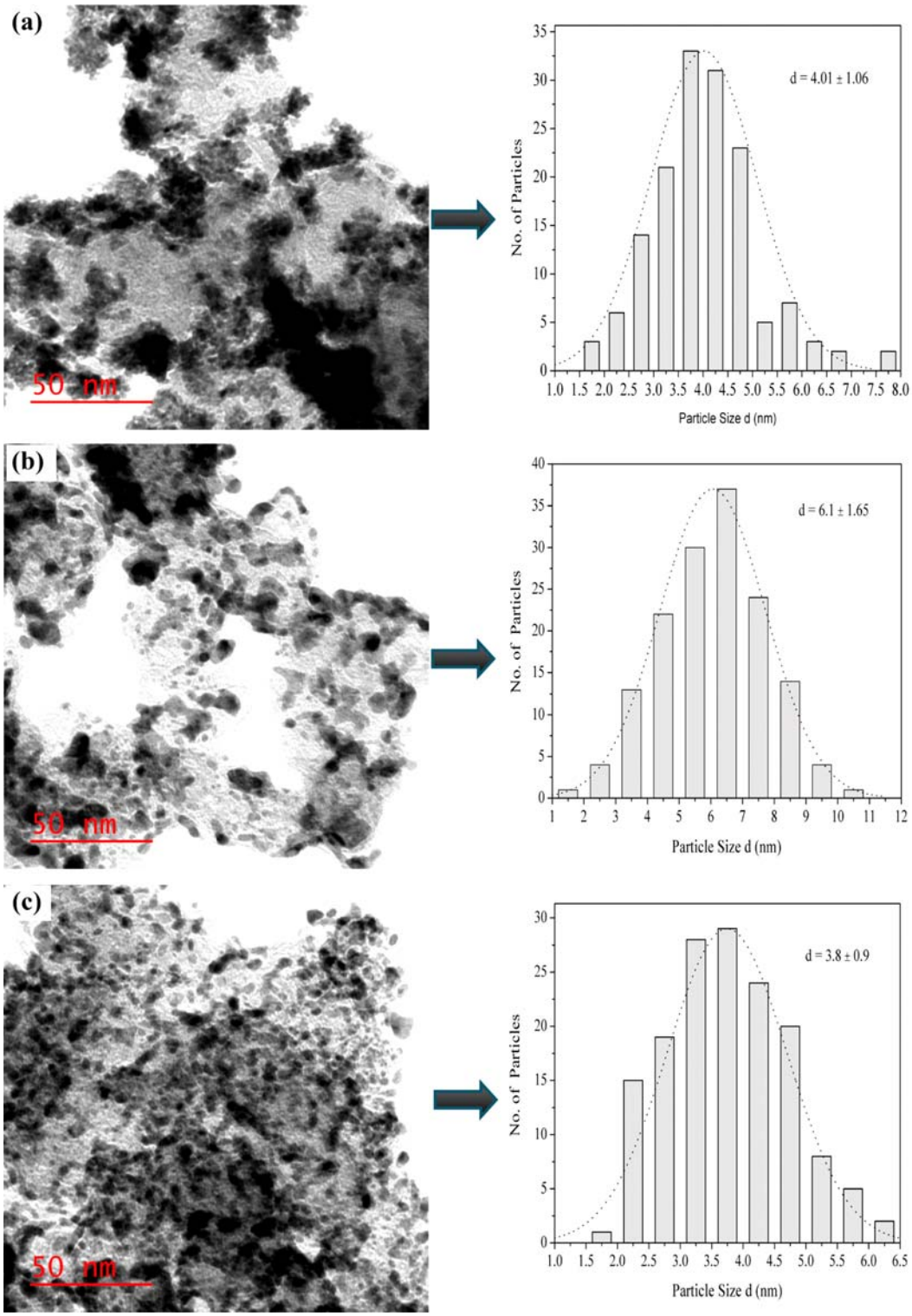


**Fig. 8. TEM images and histograms of metal particle size distribution of (a) Pt-Ru/$C_{PAB}$-PLM, (b) Pt-Ru/$C_{PAB}$-FAM, (c) Pt-Ru/$C_{AB}$-PLM, (d) Pt-Ru/$C_{AB}$-FAM and (e) commercial Pt-Ru/C electrocatalysts.**

an arbitrarily chosen area of the corresponding TEM images. A thorough analysis of TEM images depicts that the electrocatalysts consist of almost spherical shape nanosized particles, well dispersed with negligible agglomerations on the carbon support material. It is also observed in the TEM images that the metal particle size of each sample is less than 11 nm and slightly agglomerated irrespective of the electrocatalysts types (Table 4). Also from Table 4, around 18.66% of Pt-Ru/$C_{AB}$-PLM particles are present in the synthesized electrocatalyst mass with an average particle size of 3.8±0.9 nm. For Pt-Ru/$C_{AB}$-FAM synthesized electrocatalyst, about 25.33% parti-

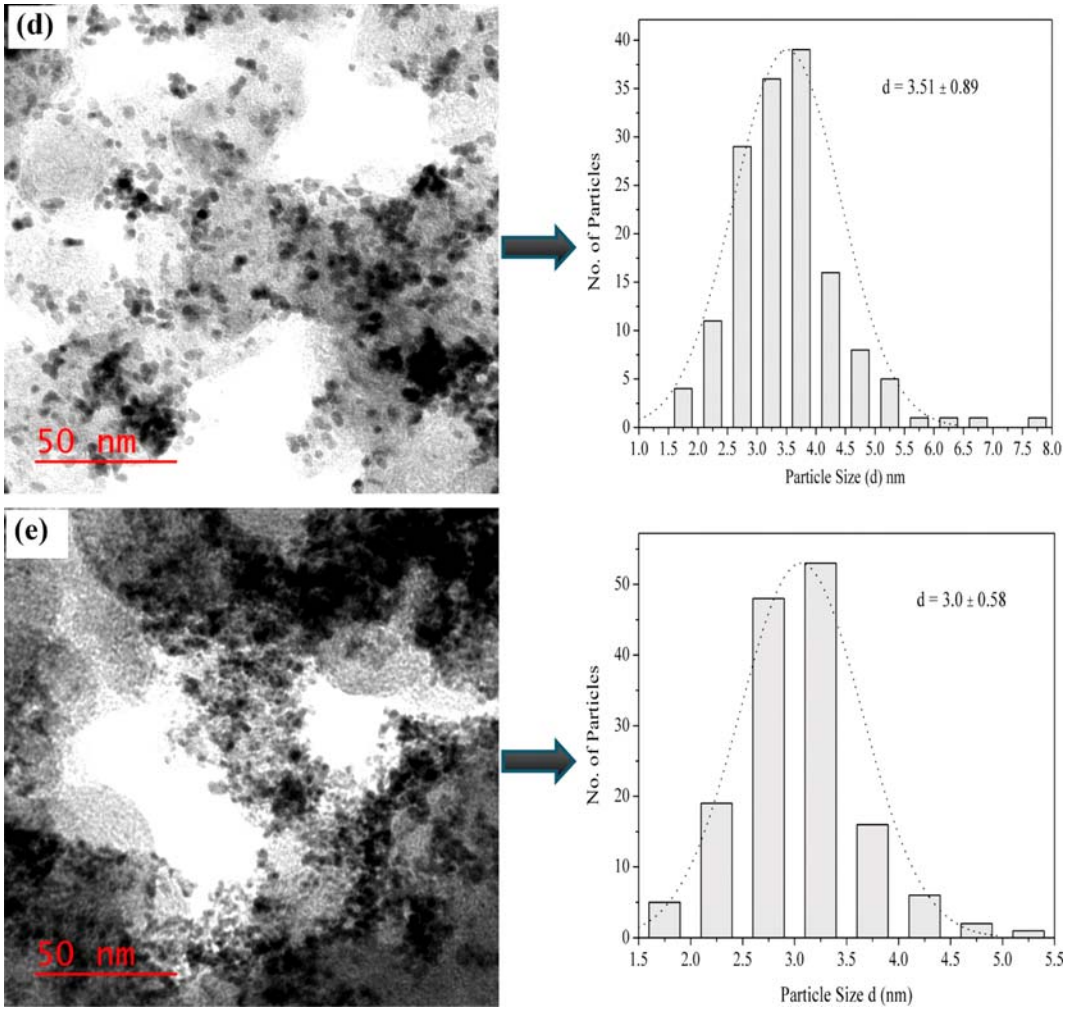


**Fig. 8. Continued.**

cle mass are present with an average particle size of 3.51±0.89 nm. Whereas, about 35.33% particles mass of commercial Pt-Ru/C electrocatalyst are present with an average particle size of 3.0±0.58 nm.

However, TEM analyses of the synthesized electrocatalysts supported on pristine acetylene black $C_{PAB}$ show similar trend in terms of size, as it is seen in the XRD analysis. For the synthesized Pt-Ru/$C_{PAB}$-PLM electrocatalyst, about 20.67% particles mass are present with an average particle size of 4.01±1.06 nm. Whereas, about 24.67% particle mass with an average particle size of 6.1±1.65 nm was found for synthesized Pt-Ru/$C_{PAB}$-FAM electrocatalyst. Metal particles in the Pt-Ru/$C_{PAB}$-PLM and Pt-Ru/$C_{PAB}$-FAM electrocatalysts are in nano range and a fraction of the metal particles clumped together to form slightly large aggregations (Fig. 8(a)-(b)).

The heavy black dots of Pt-Ru metal alloy electrocatalyst nanoparticles indicate good dispersion over carbon support lighter particles of 40-60 nm size. The particle size for Pt-Ru/$C_{AB}$-PLM synthesized catalyst ranges from 1.5 to 6.5 nm, with an average particle size of 3.8±0.9 nm. The average particle size for Pt-Ru/$C_{AB}$-FAM synthesized electrocatalyst is 3.51±0.89 nm and the size distribution is in the range of 1.5-8 nm. Similarly, for commercial Pt-Ru/C electrocatalyst, the average particle size is 3.0±0.58 nm and size distribution ranges from 1.5 to 5.5 nm. However, the average particle size for commercial Pt-Ru/C electrocatalyst is lower than syn-

**Table 4. Particle size distribution of synthesized electrocatalysts by TEM analysis**

| Type of catalysts | (%) of Particle | Particle size (nm) | No. of particles |
|---|---|---|---|
| Pt-Ru/$C_{PAB}$-PLM | 2 | 1.5-2 | 3 |
| | 4 | 2-2.5 | 6 |
| | 9.33 | 2.5-3 | 14 |
| | 14 | 3-3.5 | 21 |
| | 22 | 3.5-4 | 33 |
| | **20.67** | **4-4.5** | **31** |
| | 15.33 | 4.5-5 | 23 |
| | 3.33 | 5-5.5 | 5 |
| | 4.67 | 5.5-6 | 7 |
| | 2 | 6-6.5 | 3 |
| | 1.33 | 6.5-7 | 2 |
| | 1.33 | 7.5-8 | 2 |

**Table 4. Continued**

| Type of catalysts | (%) of Particle | Particle size (nm) | No. of particles |
|---|---|---|---|
| Pt-Ru/$C_{PAB}$-FAM | 0.66 | 1-2 | 1 |
| | 2.66 | 2-3 | 4 |
| | 8.67 | 3-4 | 13 |
| | 14.67 | 4-5 | 22 |
| | 20 | 5-6 | 30 |
| | **24.67** | **6-7** | **37** |
| | 16 | 7-8 | 24 |
| | 9.33 | 8-9 | 14 |
| | 2.67 | 9-10 | 4 |
| | 0.67 | 10-11 | 1 |
| Pt-Ru/$C_{AB}$-PLM | 1.33 | 1.5-2 | 2 |
| | 10 | 2-2.5 | 15 |
| | 14.66 | 2.5-3 | 22 |
| | 17.33 | 3-3.5 | 26 |
| | **18.66** | **3.5-4** | **28** |
| | 14.66 | 4.0-4.5 | 22 |
| | 13.66 | 4.5-5 | 20 |
| | 4.66 | 5-5.5 | 7 |
| | 3.33 | 5.5-6 | 5 |
| | 2 | 6-6.5 | 3 |
| Pt-Ru/$C_{AB}$-FAM | 2.66 | 1.5-2 | 4 |
| | 7.33 | 2-2.5 | 11 |
| | 18.66 | 2.5-3 | 28 |
| | 24 | 3-3.5 | 36 |
| | **25.33** | **3.5-4** | **38** |
| | 10.66 | 4-4.5 | 16 |
| | 5.33 | 4.5-5 | 8 |
| | 3.33 | 5-5.5 | 5 |
| | 0.66 | 5.5-6 | 1 |
| | 0.66 | 6-6.5 | 1 |
| | 0.66 | 6.5-7 | 1 |
| | 0.66 | 7.5-8 | 1 |
| Commercial Pt-Ru/C | 3.33 | 1.5-2 | 5 |
| | 12.66 | 2-2.5 | 19 |
| | 32 | 2.5-3 | 48 |
| | **35.33** | **3-3.5** | **53** |
| | 10.66 | 3.5-4 | 16 |
| | 4 | 4-4.5 | 6 |
| | 1.33 | 4.5-5 | 2 |
| | 0.66 | 5-5.5 | 1 |

thesized electrocatalysts but particles are seemed to be slightly agglomerated (Fig. 8(e)).

The average particle size estimated by TEM images and the average crystallite size by XRD analysis are almost similar to an error of ±10% (Table 5). The metal surface area of the electrocatalyst was determined using Eqs. (5) and (6), as discussed in the XRD section.

The metal surface areas (SA) obtained for synthesized Pt-Ru/$C_{PAB}$-PLM, Pt-Ru/$C_{PAB}$-FAM, Pt-Ru/$C_{AB}$-PLM and Pt-Ru/$C_{AB}$-FAM electrocatalysts are 20.46 $m^2$/g, 13.46 $m^2$/g, 22.26 $m^2$/g and 24.31 $m^2$/g respectively. The metal surface area of all synthesized electrocatalysts is slightly lower than the commercial Pt-Ru/C (25.62 $m^2$/g) electrocatalyst (Table 5). However, the surface area of synthesized Pt-Ru electrocatalyst supported on $C_{AB}$ is higher than that of the synthesized Pt-Ru supported on $C_{PAB}$. This proves that functionalized support material $C_{AB}$ resulted in smaller particle size and thus, high surface area of synthesized electrocatalysts Pt-Ru/$C_{AB}$-PLM and Pt-Ru/$C_{AB}$-FAM were observed.

2-4. XPS Analysis

The chemical oxidation/valence states and surface compositions of Pt and Ru metals in the Pt-Ru/$C_{PAB}$-PLM, Pt-Ru/$C_{PAB}$-FAM, Pt-Ru/$C_{AB}$-PLM, Pt-Ru/$C_{AB}$-FAM and commercial Pt-Ru/C nano electrocatalysts were analyzed by XPS analysis. The XPS is a surface sensitive method and most of the cluster atoms are surface atoms. Here it is assumed that the bulk information of the associated elements Pt, Ru, C and O in the supported electrocatalysts, i.e., Pt-Ru/$C_{AB}$ can only be obtained from the XPS analysis of the electrocatalysts. Fig. 9(a)-(e) selectively shows the Pt (4f) core regional spectra of synthesized Pt-Ru/$C_{PAB}$-PLM, Pt-Ru/$C_{PAB}$-FAM, Pt-Ru/$C_{AB}$-PLM, Pt-Ru/$C_{AB}$-FAM, and commercial Pt-Ru/C electrocatalysts. As reported in the literature, the Pt $4f_{7/2}$ and $4f_{5/2}$ peaks are deconvoluted into three sets of the spin-orbit doublets [22,40]. The first set of Pt $4f_{7/2}$ and Pt $4f_{5/2}$ doublets at 71.42-71.7 and 74.9-75.1 eV is assigned to pure metallic $Pt^0$ (zero valance) state. The second doublets set at 72.64-72.8 and 75.8-76.1 eV can be ascribed to oxidized $Pt^{2+}$ such as PtO or $Pt(OH)_2$ species, whereas the third doublets set at 73.9-74.7 and 77.2-77.9 eV are related to the $Pt^{4+}$ oxide such as $PtO_2$ species [22,41].

Obviously, different methods followed for the synthesis of electrocatalysts could result in different compositions of the oxidation states in the electrocatalyst metals present. The binding energies (BEs) of the Pt $4f_{7/2}$ component at their corresponding relative intensities were obtained from the respective mapped area of quantitative deconvoluted of peaks, and the corresponding full-width at the half-maximum (FWHM) values are presented in Table 6.

A slight shift of the $Pt^0$ (zero valance) peaks towards higher values of binding energies in comparison to that of bulk Pt (BE of Pt

**Table 5. The average particle size and specific area of electrocatalysts from TEM analysis and comparison with XRD results**

| Electrocatalysts | Average particle size ($d_p$) by TEM (nm) | Average crystallite size ($d_c$) by XRD (nm) | Surface area ($m^2$/g) |
|---|---|---|---|
| Pt-Ru/$C_{PAB}$-PLM | 4.01±1.06 | 3.8 | 20.46 |
| Pt-Ru/$C_{PAB}$-FAM | 6.1±1.65 | 5.8 | 13.46 |
| Pt-Ru/$C_{AB}$-PLM | 3.8±0.9 | 3.6 | 22.26 |
| Pt-Ru/$C_{AB}$-FAM | 3.51±0.89 | 3.4 | 24.31 |
| Commercial Pt-Ru/C | 3.0±0.58 | 2.8 | 25.62 |

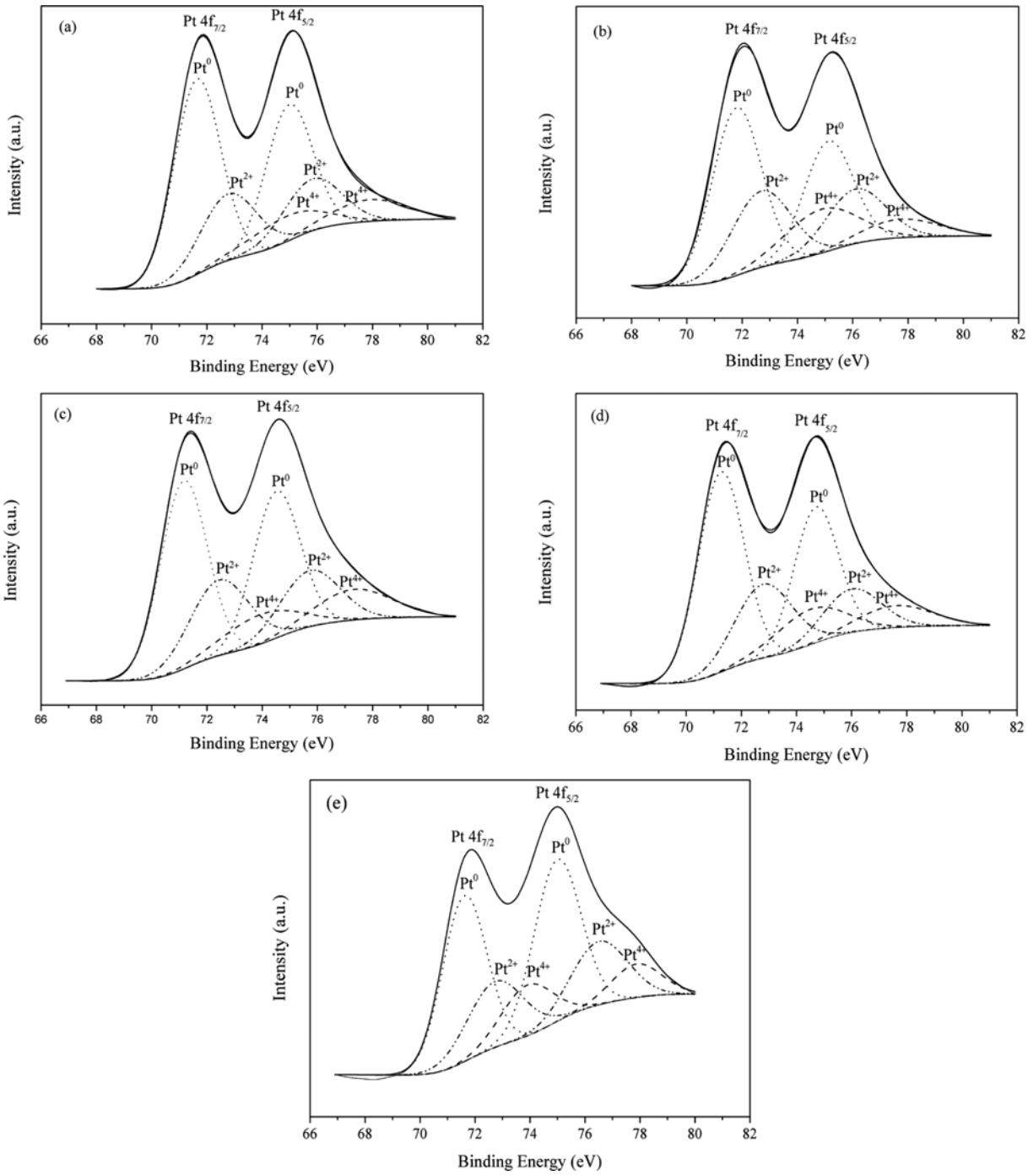


**Fig. 9. XPS spectra in Pt 4f region of (a) Pt-Ru/$C_{PAB}$-PLM, (b) Pt-Ru/$C_{PAB}$-FAM, (c) Pt-Ru/$C_{AB}$-PLM, (d) Pt-Ru/$C_{AB}$-FAM and (e) commercial Pt-Ru/C electrocatalysts. The solid line represents the XPS fitted spectra and the broken line represents the peaks due to different Pt oxidation state corresponds to $Pt^0$, $Pt^{2+}$, and $Pt^{4+}$.**

$4f_{7/2}$=70.5 eV) is due to the effect of small particles and the Pt-support interactions [22,40]. Generally, $Pt^0$ is found as only the predominant species in all the electrocatalysts (53.74-60.52%). The electrocatalysts supported on pristine acetylene black ($C_{PAB}$) and synthesized by FAM method showed the lowest amount of metallic Pt ($Pt^0$), while using same method/FAM supported on functionalized acetylene black ($C_{AB}$) exhibited the highest content of $Pt^0$. However, there is an important contribution of oxidized Pt species, such as $Pt^{2+}$/PtO or $Pt(OH)_2$ and $Pt^{4+}$/$PtO_2$. The pure metallic form is $Pt^0$, which is slightly higher in the case of Pt-Ru/$C_{AB}$-FAM compared to Pt-Ru/$C_{AB}$-PLM and commercial Pt-Ru/C electrocatalysts (Table 6). The most preferential state of Pt species, i.e., $Pt^{2+}$/PtO or $Pt(OH)_2$ was found to be maximum in the case of Pt-Ru/$C_{AB}$-PLM (28.66%) [38]. Irrespective of the synthesis methods used for electrocatalysts synthesis, the $C_{AB}$ supported electrocatalysts resulted in better oxidation state of Pt species.

**Table 6. Different oxidation states of Pt species and their relative intensities obtained from binding energies (BE) of the Pt $4f_{7/2}$ component of XPS spectra for Pt-Ru/$C_{PAB}$-PLM, Pt-Ru/$C_{PAB}$-FAM, Pt-Ru/$C_{AB}$-PLM, Pt-Ru/$C_{AB}$-FAM and commercial Pt-Ru/C electrocatalysts**

| Electrocatalysts | Pt $4f_{7/2}$ component of XPS spectra | | | |
|---|---|---|---|---|
| | Pt species | BE of $4f_{7/2}$ (eV) | FWHM (eV) | Relative intensity (%) |
| Pt-Ru/$C_{PAB}$-PLM | $Pt^0$/metallic Pt | 71.64 | 2.0 | 57.84 |
| | $Pt^{2+}$/PtO or $Pt(OH)_2$ | 72.78 | 2.5 | 27.31 |
| | $Pt^{4+}$/$PtO_2$ | 74.7 | 3.2 | 14.85 |
| Pt-Ru/$C_{PAB}$-FAM | $Pt^0$/metallic Pt | 71.7 | 2.0 | 53.74 |
| | $Pt^{2+}$/PtO or $Pt(OH)_2$ | 72.69 | 2.5 | 26.26 |
| | $Pt^{4+}$/$PtO_2$ | 74.55 | 3.1 | 20.0 |
| Pt-Ru/$C_{AB}$-PLM | $Pt^0$/metallic Pt | 71.42 | 2.0 | 57.0 |
| | $Pt^{2+}$/PtO or $Pt(OH)_2$ | 72.64 | 2.5 | 28.66 |
| | $Pt^{4+}$/$PtO_2$ | 73.95 | 3.2 | 14.34 |
| Pt-Ru/$C_{AB}$-FAM | $Pt^0$/metallic Pt | 71.47 | 2.0 | 60.52 |
| | $Pt^{2+}$/PtO or $Pt(OH)_2$ | 72.8 | 2.5 | 22.12 |
| | $Pt^{4+}$/$PtO_2$ | 74 | 3.2 | 17.36 |
| Commercial Pt-Ru/C | $Pt^0$/metallic Pt | 71.51 | 2.0 | 59.13 |
| | $Pt^{2+}$/PtO or $Pt(OH)_2$ | 72.74 | 2.5 | 27.77 |
| | $Pt^{4+}$/$PtO_2$ | 73.9 | 3.2 | 13.10 |

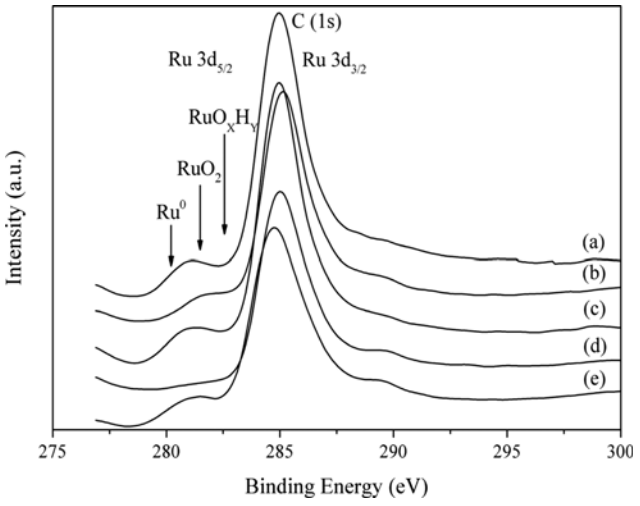


**Fig. 10. C(1s)+Ru(3d) region in (a) Pt-Ru/$C_{PAB}$-PLM, (b) Pt-Ru/$C_{PAB}$-FAM, (c) Pt-Ru/$C_{AB}$-PLM, (d) Pt-Ru/$C_{AB}$-FAM and (e) commercial Pt-Ru/C electrocatalysts.**

The XPS spectra of Ru (3d)-C(1s) region for electrocatalyst samples are presented in Fig. 10. The peak at 284.55 eV is attributed to graphitic carbon (C(1s)) supoort material in all the electrocatalysts substantiating the literature data [42,43]. A quantitative estimation of the oxidation states of Ru (3d) spectra is slightly difficult, as the C(1s) peak entirely covers the Ru($3d_{3/2}$) signal and partially overlaps with the Ru($3d_{5/2}$). However, two peaks at 280.3 eV and 281.5 eV can be easily observed for the synthesized electrocatalysts Pt-Ru/$C_{AB}$-PLM and commercial Pt-Ru/C for the Ru $3d_{5/2}$ signal as shown in Fig. 10. The peaks at 280.3 eV with a shoulder and at 281.5 eV can be qualitatively attributed to $Ru^0$ and anhydrous $RuO_2$, respectively [43,44]. However, a flat plateau is observed for Pt-Ru/$C_{AB}$-FAM in the same region. The shifting of these peaks appears at about 0.3 eV to the higher binding energies with respect to the corresponding standard values reported in the literature, which may be due to a large C1s peak tail [43]. The Ru($3d_{5/2}$) signal from hydrous amorphous $RuO_xH_y$ is predictable at a binding energy ~1 eV higher than anhydrous $RuO_2$. Hence, the overlapping of Ru($3d_{3/2}$) signal with the intense graphitic C(1s) peak, the presence of the hydrous ruthenium phase cannot be excluded. Thus, it may be concluded from the above discussion that the Pt-Ru/$C_{AB}$-PLM electrocatalyst is better than the Pt-Ru/$C_{PAB}$-PLM, Pt-Ru/$C_{PAB}$-FAM, Pt-Ru/$C_{AB}$-FAM and commercial electrocatalyst Pt-Ru/C in reference to oxidation state of Pt and Ru both.

2-5. EDX Analysis

The chemical composition of individual metal particles along with support material carbon of all the electrocatalysts was analyzed by EDX (Fig. 11(a)-(e)). The EDX patterns obviously confirm the presence of desired elements Pt, Ru, and C in the electrocatalyst. The strongest C peak is assigned to the support material in all the electrocatalysts. The electrocatalyst prepared has the desired elements with some variation in composition as reported in Table 7. The EDX results show that the elemental composition of synthesized electrocatalysts varies from point to point as the electrocatalytic surface is heterogeneous. The EDX spectrum also shows the presence of oxygen and chlorine in electrocatalysts. The presence of chlorine may be probably coming from the remains of metal precursors during the reduction process. The existence of oxygen indicates the formation of ruthenium oxides/platinum oxides which are clearly visible in XPS analysis (Table 6). The presence of these common impurities has been reported by Qian et al. and Tayal et al. [45,46].

**3. Electrochemical Characterization**

3-1. Cyclic Voltammetry

Fig. 12 shows the cyclic voltammograms (CV) of synthesized Pt-

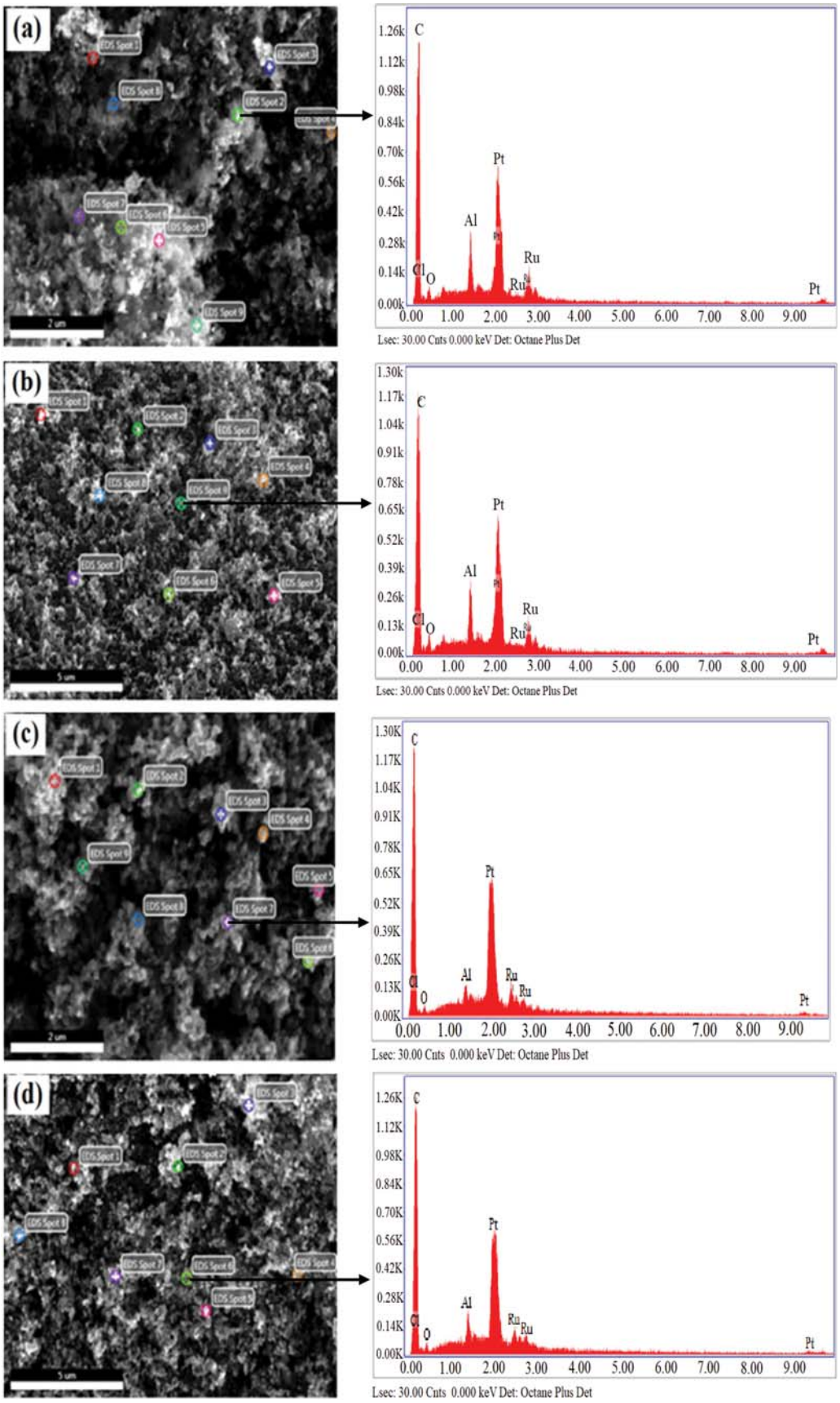


**Fig. 11. EDX pattern of (a) Pt-Ru/$C_{PAB}$-PLM, (b) Pt-Ru/$C_{PAB}$-FAM, (c) Pt-Ru/$C_{AB}$-PLM, (d) Pt-Ru/$C_{AB}$-FAM and (e) commercial Pt-Ru/C electrocatalysts.**

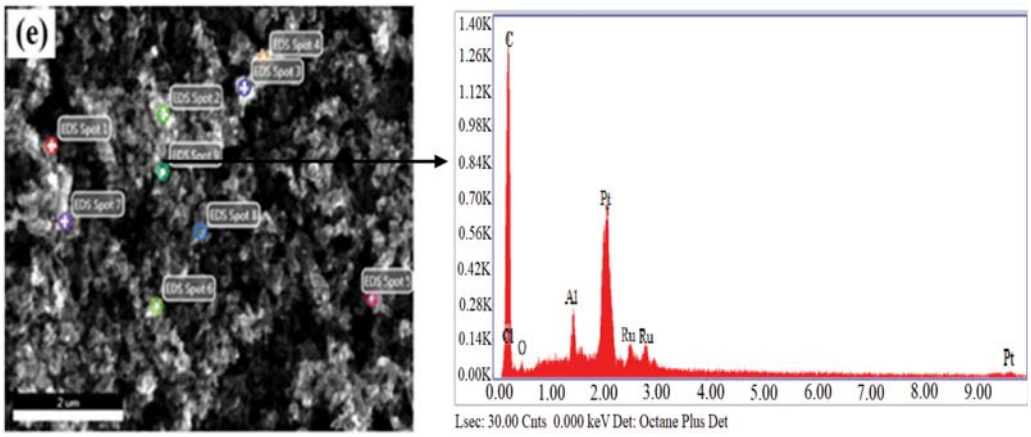


**Fig. 11. Continued.**

**Table 7. EDX results of the synthesized Pt-Ru/$C_{PAB}$-PLM, Pt-Ru/$C_{PAB}$-FAM , Pt-Ru/$C_{AB}$-PLM, Pt-Ru/$C_{AB}$-FAM and commercial Pt-Ru/C electrocatalysts**

| Electrocatalysts | Elements | Composition obtained by EDX (wt%) | Nominal composition (wt%) |
|---|---|---|---|
| Pt–Ru/$C_{PAB}$-PLM | Pt | 25.10 | 26.35 |
| | Ru | 12.30 | 13.65 |
| | C | 62.60 | 60 |
| Pt–Ru/$C_{PAB}$-FAM | Pt | 24.70 | 26.35 |
| | Ru | 12.21 | 13.65 |
| | C | 63.09 | 60 |
| Pt–Ru/$C_{AB}$-PLM | Pt | 25.71 | 26.35 |
| | Ru | 12.93 | 13.65 |
| | C | 61.36 | 60 |
| Pt–Ru/$C_{AB}$-FAM | Pt | 25.62 | 26.35 |
| | Ru | 12.59 | 13.65 |
| | C | 61.79 | 60 |
| Commercial Pt–Ru/C | Pt | 28.58 | 30 |
| | Ru | 13.74 | 15 |
| | C | 57.68 | 55 |

Ru/$C_{AB}$-PLM, Pt-Ru/$C_{AB}$-FAM and commercial Pt-Ru/C electrocatalysts for ethanol oxidation using 1 M of $C_2H_5OH$ mixed in 0.5 M of $HClO_4$.

The electrooxidation peaks for ethanol fuel were found in the forward and backward scan as well during the CV study. In the forward scan, the electrooxidation of ethanol produced a prominent anodic peak due to the electrooxidation of freshly chemisorbed species. Fig. 12 shows that the carbonaceous adsorbed species which are formed during the forward scan are further dissociated via electrooxidation during the backward scan. The noticeable electrooxidation peaks for ethanol fuel on the electrocatalysts Pt-Ru/$C_{PAB}$-PLM, Pt-Ru/$C_{PAB}$-FAM, Pt-Ru/$C_{AB}$-PLM, Pt-Ru/$C_{AB}$-FAM, and commercial Pt-Ru/C are presented in Table 8, including the positive peak potentials and corresponding peak current densities.

CV studies show that the ethanol electrooxidation peak current density of 32.59 mA/cm$^2$ at potential of 0.686 V was generated during forward scan for synthesized Pt-Ru/$C_{PAB}$-PLM electrocatalyst, while Pt-Ru/$C_{AB}$-PLM produced little higher peak current density of 34.71 mA/cm$^2$ at peak potential of 0.671 V. Similarly, a peak current density of 14.46 mA/cm$^2$ at a peak potential of 0.805 V was observed for the synthesized Pt-Ru/$C_{PAB}$-FAM electrocatalyst, while the electrooxidation peak current density of 19.05 mA/cm$^2$ was observed for Pt-Ru/$C_{AB}$-FAM at a peak potential of 0.651 V. The CV studies show that the synthesized Pt-Ru supported on functionalized $C_{AB}$ carbon support resulted in better electrocatalytic performance due to their excellent activity in comparison to pristine $C_{PAB}$ carbon supported electrocatalyst.

The onset potential of ethanol electrooxidation on all synthesized electrocatalysts Pt-Ru/$C_{AB}$-PLM and Pt-Ru/$C_{AB}$-FAM showed a shift in potential of 0.115 V and 0.135 V towards less positive in comparison to commercial Pt-Ru/C electrocatalyst. It is observed from Fig. 12 and Table 8 that the ethanol electrooxidation peak potential during forward scan of synthesized Pt-Ru/$C_{AB}$-PLM and Pt-Ru/$C_{AB}$-FAM are in the lowest potential 0.671 V and 0.651 V in comparison to commercial electrocatalyst Pt-Ru/C (0.786 V). It indicates that the loss in potential or overvoltage is low for the syn-

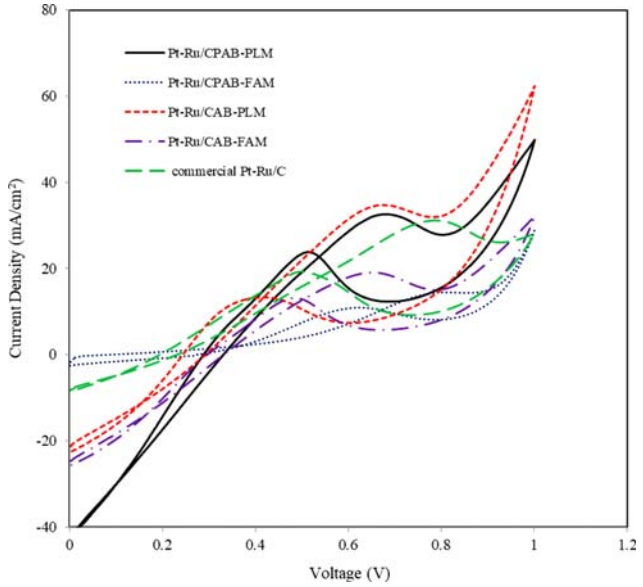


**Fig. 12. CV characteristics of the synthesized Pt-Ru/$C_{PAB}$-PLM, Pt-Ru/$C_{PAB}$-FAM, Pt-Ru/$C_{AB}$-PLM, Pt-Ru/$C_{AB}$-FAM and commercial Pt-Ru/C electrocatalysts. in 0.5 M $HClO_4$ and 1 M ethanol solution at scan rate of 20 mV/s; Temperature 35 °C.**

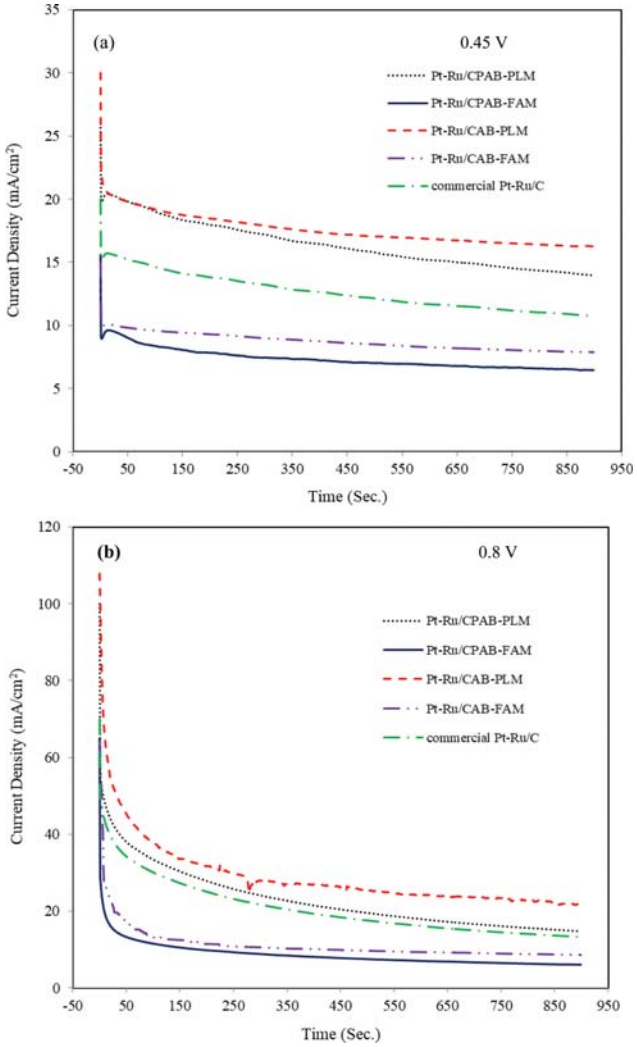


**Fig. 13. CA test of ethanol oxidation in 0.5 M perchloric acid ($HClO_4$) containing 1 M ethanol ($C_2H_5OH$) solution on synthesized Pt-Ru/$C_{PAB}$-PLM, Pt-Ru/$C_{PAB}$-FAM, Pt-Ru/$C_{AB}$-PLM, Pt-Ru/$C_{AB}$-FAM and commercial Pt-Ru/C electrocatalysts at (a) 0.45 V vs. Ag/AgCl (b) 0.8 V vs. Ag/AgCl at room temperature 35 °C.**

thesized Pt-Ru/$C_{AB}$-PLM and Pt-Ru/$C_{AB}$-FAM electrocatalyst. In addition, peak current density is highest (34.71 mA/cm$^2$) for Pt-Ru/$C_{AB}$-PLM and thus possesses the highest catalytic activity towards ethanol oxidation among all anode the electrocatalysts tested. It may be due to better alloying of Ru with Pt atom, which plays a very crucial role in electrooxidation of ethanol fuel, and this has already been discussed in XRD analysis. During the backward scan the Pt-Ru/$C_{AB}$-PLM electrocatalyst resulted in electrooxidation of adsorbed species at very low potential of 0.419 V (Eq. (2)).

In the CV study, the ethanol electrooxidation activity of anode electrocatalysts increased in the following order: Pt-Ru/$C_{PAB}$-FAM< Pt-Ru/$C_{AB}$-FAM<commercial Pt-Ru/C<Pt-Ru/$C_{PAB}$-PLM<Pt-Ru/$C_{AB}$-PLM on the basis of their peak current densities (Table 8). The Pt-Ru/$C_{AB}$-PLM electrocatalyst synthesized by polyol reduction method and supported on functionalized carbon $C_{AB}$ exhibits the most activity.

3-2. Chronoamperometry

Chronoamperometry tests of electrocatalysts can provide clues to the rate of surface poisoning or stability loss under certain test condition. The main aim here is to check if there is a rapid poisoning of the electrocatalyst upon ethanol electrooxidation. Chronoamperometry tests for the ethanol electrooxidation at different

**Table 8. CV results of the synthesized Pt-Ru/$C_{PAB}$-PLM, Pt-Ru/$C_{PAB}$-FAM, Pt-Ru/$C_{AB}$-PLM, Pt-Ru/$C_{AB}$-FAM and commercial Pt-Ru/C electrocatalysts at 20 mV/s sweep rate for ethanol electrooxidation**

| Anode electrocatalyst | Forward scan | | Backward scan | |
|---|---|---|---|---|
| | Peak potential (V vs. Ag/AgCl) | Peak current density (mA/cm$^2$) | Peak potential (V vs. Ag/AgCl) | Peak current density (mA/cm$^2$) |
| Pt-Ru/$C_{PAB}$-PLM | 0.686 | 32.59 | 0.512 | 23.82 |
| Pt-Ru/$C_{PAB}$-FAM | 0.805 | 14.46 | 0.626 | 10.95 |
| Pt-Ru/$C_{AB}$-PLM | 0.671 | 34.71 | 0.419 | 13.30 |
| Pt-Ru/$C_{AB}$-FAM | 0.651 | 19.05 | 0.483 | 13.15 |
| Commercial Pt-Ru/C | 0.786 | 31.15 | 0.500 | 19.31 |

potentials were carried out at an ethanol concentration of 1 M ethanol mixed with 0.5 M $HClO_4$ and the results are listed in Fig. 13(a)-(b). It can be clearly observed that currents for ethanol electrooxidation on all the electrocatalysts dropped rapidly and then became relatively stable. The dramatic decrease can be ascribed to diffusion effects and the gradual decrease to the poisoning of electrocatalysts due to the formation of intermediates during ethanol electro-oxidation. The reference potential (0.8 V and 0.45 V) for chronoamperometry test was obtained from C.V results (Fig. 12). It is found that at a lower potential of 0.45 V (Fig. 13(a)), the current for ethanol oxidation on Pt-Ru/$C_{AB}$-PLM electrocatalyst is significantly higher than on all the other electrocatalysts. Similarly, at the higher potential of 0.8 V (Fig. 13(b)), the electrooxidation current on Pt-Ru/$C_{AB}$-PLM synthesized electrocatalyst is always higher in comparison to synthesized Pt-Ru/$C_{PAB}$-PLM, Pt-Ru/$C_{PAB}$-FAM, Pt-Ru/$C_{AB}$-FAM and commercial Pt-Ru/C electrocatalysts.

## 4. DEFC Study

### 4-1. Performance Comparison Between Synthesized and Commercial Electrocatalysts

The electrocatalytic activity of the synthesized and commercial electrocatalysts was tested in a DEFC single cell setup, which is presented in Fig. 14. Electrocatalyst loading at the anode was 1 mg/cm$^2$ of synthesized Pt-Ru/$C_{PAB}$-PLM, Pt-Ru/$C_{PAB}$-FAM, Pt-Ru/$C_{AB}$-PLM, Pt-Ru/$C_{AB}$-FAM, and commercial Pt-Ru/C electrocatalysts, respectively. The cathode was made of commercial Pt/$C_{HiSPEC}$ of fixed loading, i.e., 1 mg/cm$^2$. The electrolyte used was a commercial Nafion® 117 membrane. The DEFC was operated at 35 °C, which was kept similar to that of CV experiments performed. As observed in CV experiments (Fig. 12), Pt-Ru/$C_{AB}$-PLM resulted in a comparable performance with the commercial Pt-Ru/C electrocatalyst in the DEFC test also (Fig. 14).

Table 9 shows the optimum values of single cell output, e.g., open circuit voltage (OCV), power density and current density as a comparative performance of the electrocatalysts in the DEFC test.

It is observed from the single cell study, the synthesized electrocatalysts supported on functionalized carbon support ($C_{AB}$) resulted in enhanced cell performance in comparison to pristine carbon support ($C_{PAB}$) while adopting the same synthesis method. Moreover, electrocatalyst synthesized via PLM method always showed better performance in terms of current and power density than any other electrocatalysts tested in the present DEFC. The maximum OCV of 0.71 V was obtained for Pt-Ru/$C_{AB}$-PLM, which is nearly about same as that of the commercial Pt-Ru/C (0.717 V) electrocatalyst. Synthesized electrocatalyst Pt-Ru/$C_{AB}$-FAM produced relatively lower OCV 0.685 V than Pt-Ru/$C_{AB}$-PLM and commercial Pt-Ru/C (0.717 V) electrocatalyst. The DEFC constructed with synthesized Pt-Ru/$C_{AB}$-PLM anode electrocatalyst yielded maximum power density of 6.02 mW/cm$^2$, which is higher than with commercial Pt-Ru/C electrocatalyst (5.13 mW/cm$^2$) and with synthesized Pt-Ru/$C_{AB}$-FAM electrocatalyst (4.54 mW/cm$^2$). For both Pt-Ru/$C_{PAB}$-PLM and Pt-Ru/$C_{PAB}$-FAM electrocatalysts, the maximum power density of 5.47 mW/cm$^2$ and 3.85 mW/cm$^2$ was obtained at a current density of 19.20 mA/cm$^2$ and 15.20 mA/cm$^2$, respectively (Table 9). After treatment of pristine acetylene black, there was an increase in OCV of Pt-Ru/$C_{AB}$-PLM and Pt-Ru/$C_{AB}$-FAM anode electrocatalysts, which indicates a difference in ethanol electrooxidation reaction mechanism due to presence of oxygenated surface groups at surface of functionalized carbon $C_{AB}$ as explained in FTIR section [31].

A rapid fall in cell voltage was observed for all electrocatalysts, which may be due to the slow initial ethanol electrooxidation reaction at the electrode surface. Moreover, metal particles were well dispersed on polyol method synthesized electrocatalyst (Pt-Ru/$C_{AB}$-PLM) and thus showed better performance to commercial Pt-Ru/C electrocatalyst. Enhanced performance of Pt-Ru/$C_{AB}$-PLM synthesized electrocatalyst could also be attributed to the positive effect of functionalized acetylene black ($C_{AB}$) as a support having high

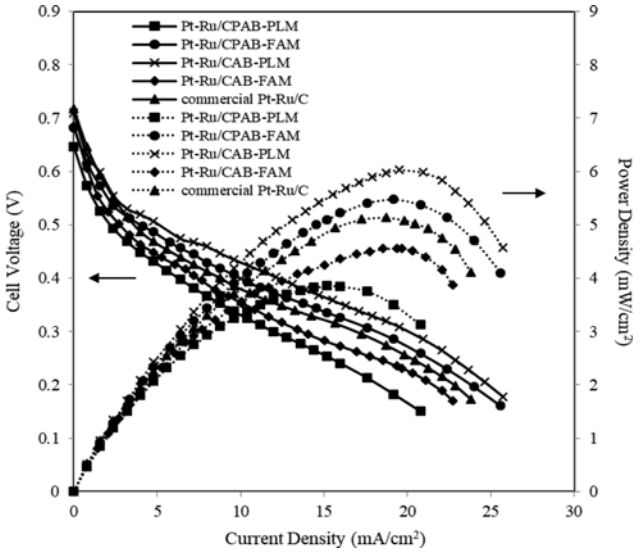


**Fig. 14. Single cell performance characteristics for different anode electrocatalysts for anode feed of 1 M ethanol. Cathode feed: humidified pure oxygen; $P_{cathode}$=1 bar (absolute); Solid line-polarization curves; Dotted line-power density curves.**

**Table 9. Summary of performance of different anode electrocatalysts in single fuel cell tests for 1 M ethanol at a cell temperature of 35 °C**

| Anode electrocatalyst | Open circuit voltage (V) | Maximum power density (mW/cm$^2$) | Current density at maximum power density (mA/cm$^2$) |
|---|---|---|---|
| Pt-Ru/$C_{PAB}$-PLM | 0.682 | 5.47 | 19.20 |
| Pt-Ru/$C_{PAB}$-FAM | 0.646 | 3.85 | 15.20 |
| Pt-Ru/$C_{AB}$-PLM | 0.71 | 6.02 | 19.52 |
| Pt-Ru/$C_{AB}$-FAM | 0.685 | 4.54 | 18.60 |
| Commercial Pt-Ru/C | 0.717 | 5.13 | 18.70 |

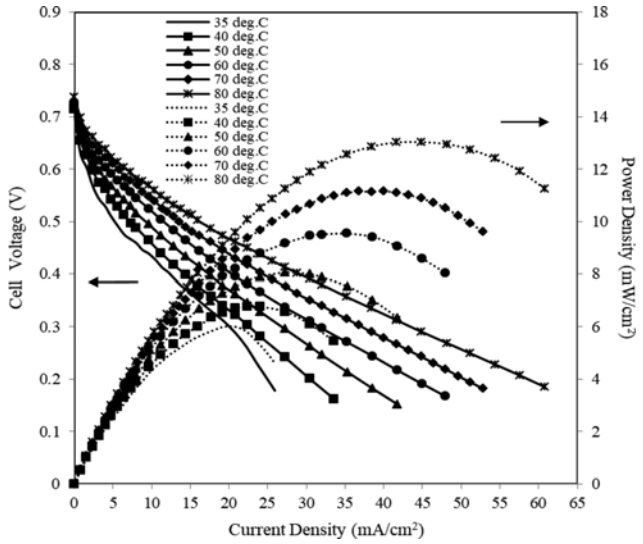


**Fig. 15. Single cell performance characteristics for varying cell temperatures using anode feed of 1 M ethanol solution. Cathode feed: pure humidified oxygen; $P_{cathode}$=1 bar (absolute); Dotted line-power density curves; Solid line-polarization curves.**

electrical conductivity, large pore volume, and more uniform distribution of the ionomer in the anode electrocatalyst layer which could result in enhanced ethanol electrooxidation kinetics to give highest current density of 19.52 mA/cm$^2$. The XPS results also predicted the better performance for synthesized Pt-Ru/C-PLM electrocatalysts (Fig. 9).

4-2. Pt-Ru/$C_{AB}$-PLM Performance at Various Temperatures

The effect of temperature on cell performance was carried out for the synthesized electrocatalyst Pt-Ru/$C_{AB}$-PLM only, as it produces highest power density at room temperature of 35 °C. Fig. 15 illustrates the effect of cell temperatures using the synthesized Pt-Ru/$C_{AB}$-PLM of 1 mg/cm$^2$ as the anode and Pt/$C_{HiSPEC}$ as cathode electrocatalyst, respectively. It is observed in Fig. 15 that the maximum power density and current density both increases with the increase in temperature up to 80 °C. Note that the maximum cell temperature was maintained at 80 °C in view of the boiling point of ethanol of about 78.4 °C. The temperature dependence of cell performance indicates that ethanol electrooxidation kinetics on synthesized Pt-Ru/$C_{AB}$-PLM electrocatalyst is thermally activated. It is reported in the literature that high temperature not only reduces activation overpotential but ohmic and concentration overpotential also. At high temperature (T<80 °C), proton conductivity of Nafion® membrane was significantly improved, which resulted in decreased ohmic polarization [47]. Additionally, high operating temperature of cell operation also favors the mass transfer rate of the reactant, thus decreasing the concentration overpotential [48]. The OCV of the single DEFC also increases due to the positive effect of temperature, and this could be explained by the Nernst equation [49]. The maximum power density of 6.02 mW/cm$^2$ at a current density of 19.52 mA/cm$^2$ was obtained when the cell was functioning at room temperature of 35 °C. However, DEFC performance was improved significantly at the highest operating tem-

**Table 10. DEFC single cell MEA performance comparison of laboratory synthesized electrocatalyst in the literature with Pt-Ru/C electrocatalysts with Nafion membrane in acidic media**

| References | Electrolyte and electrocatalyst | Other operating conditions | Maximum power density (mW/cm$^2$) | OCV (V) |
|---|---|---|---|---|
| Zhou et al. [11] | Nafion® 115;<br>Anode: Pt-Ru (Pt 20 wt%, Pt : Ru=1 : 1)/ C (1.33 mg Pt/cm$^2$);<br>Cathode: Pt (20 wt%)/C (1 mg/cm$^2$) (JM) | Fuel: ethanol (1 M) (1.0 ml/min);<br>Oxidant: unhumidified $O_2$ (120 ml/min);<br>Temperature: 90 °C | 28.54 | 0.677 |
| Colmati et al. [8] | Nafion® 115;<br>Anode: Pt-Ru (20 wt%, Pt : Ru=1 : 1)/ C (1 mg Pt/cm$^2$) (E-TEK);<br>Cathode: Pt (20 wt%)/ C (1 mg Pt/cm$^2$) (E-TEK) | Fuel: ethanol (1 M);<br>Oxidant: $O_2$;<br>Temperature: 80 °C | 10.5 | 0.65 |
| Fatih et al. [10] | Nafion® 117;<br>Anode: Pt-Ru (1 : 1)/ C-HISPEC 5000 (2 mg/cm$^2$) (JM);<br>Cathode: Pt (60 wt%)/C (2 mg/cm$^2$) (JM) | Fuel: ethanol (1 M) (2 ml/min);<br>Oxidant: $O_2$ (300 ml/min);<br>Temperature: 90 °C | 12.0 | 0.69 |
| Figueiredo et al. [50] | Nafion® 115;<br>Anode: Pt-Ru (40% : 20% by wt)/ C (2.32 mg/cm$^2$) (AA);<br>Cathode: Pt (60 wt%)/C (2 mg/cm$^2$) (AA) | Fuel: ethanol (1 M) (1.5 ml/min);<br>Oxidant: humidified $O_2$ (200 ml/min);<br>Temperature: 70 °C | 12.10 | 0.70 |
| Present work | Nafion® 117;<br>Anode: Pt-Ru (1 : 1)/$C_{AB}$-PLM (1 mg/cm$^2$);<br>Cathode: Pt (40 wt%)/C (1 mg/cm$^2$) (AA) | Fuel: ethanol (1 M) (1.2 ml/min);<br>Oxidant: humidified $O_2$ (60 ml/min);<br>Temperature : 80 °C | 13.04 | 0.735 |

*JM-Johnson Matthey, AA-Alfa Aesar

perature of 80 °C. The maximum power density of 13.04 mW/cm$^2$ at a current density of 44.8 mA/cm$^2$ was achieved at this temperature (80 °C). A noticeable increase in the power density, i.e., about 117% was achieved for the temperature increase from 35 °C to 80 °C.

4-3. Performance Comparison of Pt-Ru/$C_{AB}$-PLM with Literature Reported Pt-Ru/C

The fuel cell performance using laboratory synthesized Pt-Ru nano electrocatalyst supported on functionalized acetylene black carbon ($C_{AB}$) is very promising in comparison to the research work published in the literature [8,10,11,50]. Table 10 shows the performance of literature reported DEFC single cell performance using Pt-Ru/C as anode electrocatalysts and comparison of the same with laboratory synthesized best electrocatalyst Pt-Ru/$C_{AB}$-PLM. Zhou et al. [11] performed electrooxidation of ethanol on Pt-Ru/C (Pt 20 wt%, Pt : Ru=1 : 1) electrocatalyst synthesized by ethylene glycol reduction method. The maximum power density of 28.54 mW/cm$^2$ and OCV of 0.677 V was obtained at 90 °C. The better performance of DEFC may be due to the high electrocatalyst loading (1.33 mg Pt/cm$^2$) and high operating temperature (90 °C). Colmati et al. [8] obtained maximum power density of 10.5 mW/cm$^2$ and OCV of 0.65 V using commercial Pt-Ru/C (E-TEK) as anode electrocatalyst at a DEFC temperature of 80 °C. The OCV (0.65 V) and power density (10.5 mW/cm$^2$) both were comparatively lower than in the present work. Fatih et al. [10] studied DEFC using Nafion® 117 as electrolyte and commercial Pt-Ru/C as anode electrocatalyst (2 mg/cm$^2$) at 90 °C. The maximum power density of 12.0 mW/cm$^2$ and OCV of 0.69 V was obtained. Although, the DEFC temperature and anode electrocatalyst loading were high, the cell performance was slightly low. Figueiredo et al. [50] used the commercial Pt-Ru (40% : 20% by wt)/C as anode electrocatalyst (2.32 mg/cm$^2$) at 70 °C and reported peak power density of 12.10 mW/cm$^2$ and OCV of 0.70 V. However, in our present study, the maximum power density of 13.04 mW/cm$^2$ and OCV of 0.735 V was obtained for 1 M ethanol at the cell temperature of 80 °C using synthesized Pt-Ru/$C_{AB}$-PLM (1 mg/cm$^2$) as anode. Undoubtedly, the present DEFC performance is comparable with the published works and in some cases a little better.

## CONCLUSIONS

A highly conductive, low cost and functionalized acetylene black carbon ($C_{AB}$) was manufactured in laboratory and used as support material for synthesis of Pt-Ru bi-metallic nano electrocatalysts. The TEM and SEM analyses indicate that the electrocatalysts consist of highly dispersed nano-sized (1.5-8 nm) metal particles, are spherical shaped and slightly agglomerated. The size of metal nano particles and their distribution over the support material are strongly influenced by the synthesis method used to prepare the electrocatalysts in a fuel cell. The polyol reduction method (PLM) resulted in little large metal crystallite sizes in comparison to formic acid reduction method (FAM). However, Ru alloying with Pt metal was more (37%) for PLM reduction. The EDX and XRD analyses confirm the formation Pt-Ru electrocatalysts supported on functionalized acetylene black carbon ($C_{AB}$) having a typical Pt crystalline structure and the formation of better Pt-Ru alloy. The pristine acetylene black ($C_{PAB}$) supported electrocatalyst exhibited poor electrocatalytic activity for ethanol electroxidation. The XRD analysis confirmed that the addition of the smaller atomic sized Ru could result in the contraction of Pt lattice parameter. The EDX analysis highlights the presence of all desired elements like Pt, Ru as active metal sites and C as support, respectively. The synthesized electrocatalysts based on functionalized acetylene black carbon ($C_{AB}$) were also notably more active for electrooxidizing ethanol than a commercial electrocatalyst, commonly employed as anodes in DEFCs, which can also be attributed to the positive effect of functionalized acetylene black ($C_{AB}$) as a support having high electrical conductivity and large pore volume as mentioned earlier. The CV results and chronoamperometry test of synthesized Pt-Ru/$C_{AB}$-PLM for ethanol electrooxidation in a half cell also substantiated the DEFC results with similar conditions. The synthesized Pt-Ru/$C_{AB}$-PLM electrocatalyst produced highest power density of 6.02 mW/cm$^2$, which is even higher than that of commercial Pt-Ru/C (5.13 mW/cm$^2$) electrocatalyst at the room temperature of 35 °C. The power density of the cell increased around 117% when cell temperature was raised to 80 °C for the anode electrocatalyst Pt-Ru/$C_{AB}$-PLM. Thorough analyses and performance of synthesized electrocatalysts indicate that the Pt-Ru/$C_{AB}$-PLM could be used as an alternative to commercial Pt-Ru/C electrocatalyst, especially for ethanol electrooxidation. Note that the cost of synthesized electrocatalyst is about half of the commercial electrocatalyst cost.

The synthesized Pt-Ru/$C_{AB}$-PLM could be modified further by changing metal ratio of Pt to Ru for improving its electrocatalytic activity towards the electrooxidation of ethanol fuel at low temperature and low electrocatalyst loading. Moreover, tri-metallic electrocatalysts such as Pt-Ru-X/C (where, X=Re, Rh, Sn and Ni etc.) supported on functionalized acetylene black ($C_{AB}$) could be synthesized to enhance the ethanol electrooxidation kinetics, which would result in better DEFC performance in terms of current density and power density.

## REFERENCES

1. H. Liu, C. Song, L. Zhang, J. Zhang, H. Wang and D. P. Wilkinson, *J. Power Sources*, **155**, 95 (2006).
2. E. Antolini, *J. Power Sources*, **170**, 1 (2007).
3. H. Huang and X. Wang, *J. Mater. Chem., A*, **2**, 6266 (2014).
4. H. Pramanik and S. Basu, *Can. J. Chem. Eng.*, **85**, 781 (2007).
5. H. Pramanik, S. Basu and A. A. Wragg, *J. Appl. Electrochem.*, **38**, 1321 (2008).
6. C. Lamy, A. Lima, V. LeRhun, F. Delime, C. Coutanceau and J.-M. Leger, *J. Power Sources*, **105**, 283 (2002).
7. A. K. Rathoure and H. Pramanik, *Int. J. Hydrogen Energy*, **41**, 15287 (2016).
8. F. Colmati, E. Antolini and E. R. Gonzalez, *J. Power Sources*, **157**, 98 (2006).
9. L. Colmenares, H. Wang, Z. Jusys, L. Jiang, S. Yan, G. Q. Sun and R. J. Behm, *Electrochim. Acta*, **52**, 221 (2006).
10. K. Fatih, V. Neburchilov, V. Alzate, R. Neagu and H. Wang, *J. Power Sources*, **195**, 7168 (2010).
11. W. Zhou, Z. Zhou, S. Song, W. Li, G. Sun, P. Tsiakaras and Q. Xin, *Appl. Catal. B*, **46**, 273 (2003).

12. P. E. Tsiakaras, *J. Power Sources*, **171**, 107 (2007).
13. M. J. Lázaro, V. Celorrio, L. Calvillo, E. Pastor and R. Moliner, *J. Power Sources*, **196**, 4236 (2011).
14. S. Samad, K. S. Loh, W. Y. Wong, T. K. Lee, J. Sunarso, S. T. Chong and W. R. Daud, *Int. J. Hydrogen Energy*, **43**, 7823 (2018).
15. K. Wikander, H. Ekstrom, A. E. C. Palmqvist, A. Lundblad, K. Holmberg and G. Lindbergh, *Fuel Cells*, **6**, 21 (2006).
16. Y. Shao, G. Yin, J. Zhang and Y. Gao, *Electrochim. Acta*, **51**, 5853 (2006).
17. M. Uchida, Y. Fukuoka, Y. Sugawara, N. Eda and A. Ohta, *J. Electrochem. Soc.*, **143**, 2245 (1996).
18. K. Han, J. Lee and H. Kim, *Electrochim. Acta*, **52**, 1697 (2006).
19. M. Zhiani, J. Jalili, B. Rezaei and M. M. Taghiabadi, *Int. J. Hydrogen Energy*, **38**, 5419 (2013).
20. N. Lakshmi, N. Rajalakshmi and K. S. Dhathathreyan, *J. Phys. D Appl. Phys.*, **39**, 2785 (2006).
21. K.-S. Lee, H.-Y. Park, Y.-H. Cho, I.-S. Park, S. J. Yoo and Y.-E. Sung, *J. Power Sources*, **195**, 1031 (2010).
22. E. Lee, A. Murthy and A. Manthiram, *Electrochim. Acta*, **56**, 1611 (2011).
23. G. Álvarez, F. Alcaide, O. Miguel, L. Calvillo, M. J. Lázaro, J. J. Quintana, J. C. Calderón and E. Pastor. *J. Solid State Electrochem.*, **14**, 1027 (2010).
24. V. M. Nikolić, D. L. Žugić, A. D. Maksić, D. P. Šaponjić and M. P. Kaninski, *Int. J. Hydrogen Energy*, **36**, 11004 (2011).
25. J. G. de La Fuente, M. Martinez-Huerta, S. Rojas, P. Hernandez-Fernandez, P. Terreros, J. L. Fierro and M. A. Peña, *Appl. Catal. B: Environ.*, **88**, 505 (2009).
26. K.-J. Huang, J.-Z. Zhang, Y. L. Jia, K. Xing and Y.-M. Liu, *J. Alloys Compd.*, **641**, 119 (2015).
27. J. J. Tang, J. Yang, X. Y. Zhou, J. Xie and G. H. Chen, *Micropor. Mesopor. Mater.*, **143**, 54 (2014).
28. C. Zu, Y.-S. Su and Y. Fu, *Phys. Chem. Chem. Phys.*, **15**, 2291 (2013).
29. L.-X. Miao, W.-K. Wang, M. J. Wang, A.-B. Wang, K.-G. Yuan and Y.-S. Yang, *J. Mater. Chem. A*, **1**, 11659 (2013).
30. G. Jin, Z. Mingang, Y. Shijian, Y. Xiaoyan and W. Shiwei, *Ionics*, **24**, 2219 (2018).
31. J. Goel and S. Basu, *Int. J. Hydrogen Energy*, **39**, 15956 (2014).
32. B. Yang, Q. Lu, Y. Wang, L. Zhuang, J. Lu and P. Liu, *Chem. Mater.*, **15**, 3552 (2003).
33. J. Datta, S. Singh, S. Das and N. R. Bandyopadhyay, *Bull. Mater. Sci.*, **32**, 643 (2009).
34. H. Li, G. Sun, L. Cao, L. Jiang and Q. Xin, *Electrochim. Acta*, **52**, 6622 (2007).
35. E. Antolini and F. Cardellini, *J Alloy Compd.*, **315**, 118 (2001).
36. E. Antolini, F. Giorgi, F. Cardellini and E. Passalacqua, *J. Solid State Electrochem.*, **5**, 131 (2001).
37. G. Wang, T. Takeguchi, E. N. Muhamad, T. Yamanaka and W. Ueda, *Int. J. Hydrogen Energy*, **36**, 3322 (2011).
38. J. Tayal, B. Rawat and S. Basu, *Int. J. Hydrogen Energy*, **37**, 4597 (2012).
39. D. Chu and S. Gilman, *J. Electrochem. Soc.*, **143**, 1685 (1996).
40. F. I. Pires, P. G. Corradini, V. A. Paganin, E. Antolini and J. Perez, *Ionics*, **19**, 1037 (2013).
41. K. C. Park, I. Y. Jang, W. Wongwiriyapan, S. Morimoto, Y. J. Kim, Y. C. Jung, T. Toya and M. Endo, *J. Mater. Chem.*, **20**, 5345 (2010).
42. D. R. Rolison, P. L. Hagans, K. E. Swider and J. W. Long, *Langmuir*, **15**, 774 (1999).
43. A. S. Aricò, V. Baglio, A. Di Blasi, E. Modica, P. L. Antonucci and V. Antonucci, *J. Electroanal. Chem.*, **557**, 167 (2003).
44. R. K. Raman, A. K. Shukla, A. Gayen, M. S. Hegde, K. R. Priolkar, P. R. Sarode and S. Emura, *J. Power Sources*, **157**, 45 (2006).
45. Y. Qian, W. Wen, P. A. Adcock, Z. Jiang, N. Hakim, M. S. Saha and S. Mukerjee, *J. Phys. Chem.* C, **112**, 1146 (2008).
46. J. Tayal, B. Rawat and S. Basu, *Int. J. Hydrogen Energy*, **36**, 14884 (2011).
47. V. Alzate, K. Fatih and H. Wang, *J. Power Sources*, **196**, 10625 (2011).
48. J. Goel and S. Basu, *Energy Procedia*, **1**, 66 (2012).
49. J. Larminie and A. Dicks, 2nd Ed., Wiley, Sussex, 53 (2003).
50. M. C. Figueiredo, O. Sorsa, R. M. Arán-Ais, N. Doan, J. M. Feliu and T. Kallio, *J. Catal.*, **329**, 69 (2015).